MOLECULAR-DYNAMICS INVESTIGATION OF THE DYNAMIC PROPERTIES
OF Pd AND Al METALS, AND THEIR ALLOYS

A THESIS SUBMITTED TO
THE GRADUATE SCHOOL OF NATURAL AND APPLIED SCIENCES
OF
THE MIDDLE EAST TECHNICAL UNIVERSITY

BY

ALİ ÇORUH

IN PARTIAL FULFILLMENT OF THE REQUIREMENTS FOR THE DEGREE OF

DOCTOR OF PHILOSOPHY

IN

THE DEPARTMENT OF PHYSICS

DECEMBER 2003

Approval of the Graduate School of Natural and Applied Sciences.

————————————————

Prof. Dr. Canan Özgen
Director

I certify that this thesis satisfies all the requirements as a thesis for the degree of Doctor of Philosophy.

————————————————

Prof. Dr. Sinan Bilikmen
Head of Department

This is to certify that we have read this thesis and that in our opinion it is fully adequate, in scope and quality, as a thesis for the degree of Doctor of Philosophy.

————————————————

Prof. Dr. Mehmet Tomak
Supervisor

Examining Committee Members

Prof. Dr. Mehmet Tomak   ————————————————

Prof. Dr. Bülent Karasözen   ————————————————

Prof. Dr. Cevdet Tezcan   ————————————————

Prof. Dr. Bülent Akınoğlu   ————————————————

Assoc. Prof. Dr. Hatice Kökten   ————————————————

ABSTRACT

MOLECULAR-DYNAMICS INVESTIGATION OF THE DYNAMIC PROPERTIES
OF Pd AND Al METALS, AND THEIR ALLOYS

ÇORUH, Ali

Ph. D., Department of Physics

Supervisor: Prof. Dr. Mehmet Tomak

December 2003, 93 pages.

The dynamic properties of Palladium (Pd) and Aluminum (Al) metals and their
alloys are investigated by means of Molecular Dynamics using the Quantum
Sutton-Chen force field in five different concentrations. Calculations have been
carried out for liquid structures. Although this study is done for liquid struc-
tures, basic solid state properties are also investigated to prove the validity of
potential parameters. Results are compared with each other and with experi-
mental, theoretical and simulated results. Liquid state transferability of Quantum
Sutton-Chen parameters have been investigated and discussed. High temperature
properties, which are not easy to work experimentally, are simulated and high
temperature behavior of Pd-Al alloy is investigated.

Keywords: Molecular-Dynamics Simulation, Alloys, Palladium, Aluminum, Ther-
mal and Mechanical Properties, Liquid Metals, Dynamical properties.

ÖZ

PALLADYUM VE ALUMİNYUM METALLERİNİN VE ALAŞIMLARININ DİNAMİK OZELLİKLERİNİN MOLEKÜLER-DİNAMİK İNCELEMESİ

ÇORUH, Ali

Doktora, Fizik Bölümü

Tez Yöneticisi: Prof. Dr. Mehmet Tomak

Aralık 2003, 93 sayfa.

Palladyum (Pd) ve Aluminyum (Al) metallerinin ve Pd-Al metal alaşımının dinamik özellikleri, Quantum Sutton-Chen kuvvet alanı kullanılarak moleküler dinamik (MD) yöntemi ile incelendi. Hesaplamalar, sıvı yapılarında yapıldı. Bu çalışma esas olarak sıvı metaller ve metal alaşımının incelenmesi için yapılmış olmasına rağmen, potansiyel parametrelerinin geçerliliğini göstermek için temel katı özellikleri de çalışıldı. Sonuçlar birbiri ile ve yayınlanmış deneysel, teorik ve modelleme verilerle karşılaştırıldı. Quantum Sutton-Chen parametrelerinin sıvı metaller veya metal alaşımına da uygulanabilirliği tartışıldı. Deneysel olarak çalışılması kolay olmayan, yüksek teknoloji gerektiren özellikler modellenerek incelendi ve palladyumun yüksek sıcaklık tavrı izlendi.

Anahtar Kelimeler: Moleküler-Dinamik modelleme, Alaşımlar, Palladyum, Aluminyum,Termal ve Mekanik Özellikler, Sıvı Metaller, Dinamik Özellikler.

ACKNOWLEDGMENTS

I express my sincere appreciation to Prof. Dr. Mehmet Tomak for his guidance and insight throughout the research.

Special thanks to Dr. Mustafa Uludoğan for discussions and computational help, Dr. Sadi Turgut and Prof. Dr. Mustafa Savcı for editorial check, and Ph. D. student H. Hüseyin Kart for technical support.

Finally, I am deeply indebted to family for their moral support and altruisticity.

... TO MY FAMILY

TABLE OF CONTENTS

LIST OF TABLES

CHAPTER 1

INTRODUCTION

1.1   Physical properties of Palladium and Aluminum

Palladium and aluminum are very important materials both technologically
and scientifically. Many experimental, theoretical, and computational studies
have been performed on these materials. Both elements have important physical
properties.

Palladium [1] is in group VIII (subgroup C) of period V in the periodic table.
Its atomic weight is 106.7 amu, and its atomic volume is 8.37 $cm^3/g - atom$ under
normal conditions.

The position of palladium in the last column of group VIII between rhodium
and silver horizontally, and between nickel and platinum vertically, determines
its mean physico-chemical properties in the group of noble and base metals.

Palladium is a monomorphic metal, with a face centered cubic (fcc) structure.
The lattice parameter $a = 3.8830$ $\mathring{A}$, atomic diameter $= 2.7448$ $\mathring{A}$, inter-atomic
distances $= 2.7455 \mathring{A}$, ion diameter $= 1.28 \mathring{A}$, density at 20 ^oC is 12.02 g/cm^3, and
10.7 g/cm^3 in the molten state at melting point. The melting point of palladium
is 1827.15 K [1].

Palladium, like all of the platinum group noble elements, has comparatively

low electrical resistivity and high temperature coefficient of resistance. Both of these characteristics are extremely sensitive to metal purity [2].

Palladium has the lowest elastic characteristics among the platinum metals, comparatively low strength, and high reduction of area and percentage of elongation characteristics [1].

Palladium dissolves in aqua regia and nitric acid, but resist cold sulfuric acid and hydrochloric acids. Hydrofluoric acids, fused alkalis, and soda do not react with palladium [1]. It is used in jewelry industry because of this property.

Palladium is a good hydrogen trap. Palladium and hydrogen form two limited solid solutions: an α solid solution containing about 30 volumes hydrogen per volume palladium and β-solid solution contains $1023 - 1300$ volumes of hydrogen per volume of Pd [1].

Palladium is an important transition metal because of its wide usage in medicine, nano-technology, electronic, semiconductor, energy and chemistry technologies, plating and jewelry, automotive and space industry.

Palladium isotopes are being used directly as a component or as a catalyzer for medical drugs because of its high chemical interest to hydrogen. For example, palladium is widely used as a hydrogenation catalysis of lung cancer drugs in the medicine technology [4], cell differentiation, and homeostasis [5, 6, 7]. Another important usage of palladium isotopes is the radioactive prostate cancer treatment [8, 9, 10].

Using nanotechnology, researchers have developed the world's fastest and most energy-efficient hydrogen detector. The detector consists of an array of hundreds

of ultra thin metal Pd wires that become less resistant when exposed to whiffs of hydrogen. In the future, it should become a key component of motors fueled by hydrogen.

Palladium is widely used in hydrogen purifying devices. As a result, many studies are done on the hydrogen purifying properties of palladium. Membrane processes exploit the selective transmission characteristics of the membrane material for different molecules, but the most effective membranes are also the most expensive (palladium membrane). These membranes are nowadays used to some extent for highest purity in the chemical and microelectronics industries. Palladium based membranes are used to build high performance hydrogen purifier technology [11]-[16],

Palladium is used to build conducting nano-wires in electronics industry. Because good conductors (i.e., Au, Cu or Al) are not available for doping nano-wires (carbon or silicon nano-wire), they form separate clusters, and to prevent this unwanted result, palladium alloys of these materials are doped on nano-tubes [17]. Palladium is also used to build chemical processors [18, 19, 20, 21] and in plating and jewelry industry and space industries. These properties increase the importance of this rare element. Pd is investigated experimentally in many works with respect to its hydrogen synthesis behavior [15, 22, 24], environmental pollution [25], electronic properties [26], surface properties [27, 28], nano properties [29] and bulk properties [30, 31, 32].

Aluminum [3] is a group III element. It is in the same group with Na. The radius of Al atom is 1.42885 $\mathring{A}$ at 25 ^oC its atomic weight is 26,981 amu under

normal conditions.

Aluminum crystallizes with a face-centered cubic (fcc) lattice structure. The lattice constant of fcc aluminum is 4.0414 $\mathring{A}$ at 25 ^oC. Thus the smallest distance between two adjacent aluminum atoms will be 2.8577 $\mathring{A}$ at 25 ^oC. Solid state density of aluminum is 2.702 g/cm^3 at 20 ^oC and liquid state density of aluminum is 2.380 g/cm^3 at 933 K. The melting point of aluminum is 933 K.

Aluminum is used widely in industry. Plating and automotive technology are some of the many areas of usage of aluminum. Aluminum dissolves in aqua but can not resist the acidic interactions.

Besides a number of experimental studies, palladium and palladium alloys have been also investigated theoretically and computationally by using various simulation techniques [22]-[36]. The first simulation was carried out by Metropolis [37, 38] at Los Alamos laboratory in 1953. This program formed the base of Monte-Carlo simulation (MC) method by Metropolis [38, 39]. Rahman solved the equations of motion for a set of Lennard-Jones particles and established the Molecular Dynamics (MD) method [40]. Car-Parinello included electron-ion interaction and developed MD method to a more realistic first-principles level [41, 42].

Since Molecular Dynamics (MD) simulation method became one of the most powerful simulation methods, it is used in this work to investigate the physical properties of Pd, Al and their alloys in solid and liquid states. Many researchers used MD method to analyze the physical properties of metals, metal alloys, and composite molecules (i.e., melting point estimation, elastic constants calculation,

trajectories, stress dependent properties) by using various potentials [43]-[47]. It is also used to calculate advanced properties of metals, metal alloys and composite materials [48]-[55]. Detailed information about MD is given in the next chapter.

Two-body potentials are the first potentials used to describe the interaction between atoms. The class of materials which can be realistically modeled using this approach is in practice limited to rare gases, where no electrons are available for bonding and atoms are attracted toward each other only through the weak van der Waals forces [56]. Systems of more practical interest such as metals and semiconductors cannot be modeled with pairwise forces. Lennard-Jones (LJ) or Morse type potentials, which are probably the most commonly used ones, are derived originally for inert gases.

The second chapter includes a historical background of MD simulation method. The effect of number of atoms on the length of trajectory files is the first subject. It is continued by Hamilton dynamics which is the mathematical base of MD simulation[57]. Next, MD simulation at constant pressure and temperature is discussed. Extended Hamilton formalism MD at constant external stress (HPN ensemble)[58] is given under this headline. The next ensemble identified in the second section is Molecular dynamics at constant external temperature (TPN formalism) [59, 60]. MD simulation is explained in detail by molecular dynamics algorithms and Gear's predictor-corrector algorithm. Periodic boundary conditions and minimum image convention with cut-off radius is one of the solutions to simulate the system without using large amount of computational storage.

Third chapter includes a detailed information about force fields (FF) used in

this study. Finnis-Sinclair (FS) empirical many-body potential model is proposed to overcome the problems that arise in pair potentials [61]. This potential produces reasonable elastic constants for cubic metals, but in the long range limit FS potential is not enough [62]. To overcome this problem Sutton and Chen (SC) proposed a new form of FS potential, with a van der Waals tail [62]. The Sutton-Chen potential is explained in detail in the third section. SC potential is parametrized for pure and alloy case of fcc metals by Rafii-Tabar and Sutton [63] and it is used to calculate the physical properties of metal alloys with this parametrization. Kimura *et al.*[64, 65, 66] modified SC to include quantum corrections (e.g., zero-point energy) in comparing properties to experiment, leading to quantum Sutton-Chen (Q-SC) force field. Some other parametrizations of SC potential are published for some metals and metal alloys [67].

In the fourth chapter, results for solid state are discussed. Enthalpy, density and elastic constants of both metals are calculated for lower temperatures. Miscibility property of Pd and Al metals and validity of optimized parameters for solid state are discussed.

In the fifth chapter, liquid state and melting process of Pd and Al liquid metals and Pd-Al liquid metal alloys are discussed. Liquid phase properties, such as the pair distribution functions and static structure factors [57, 68, 69] are given in the fifth chapter. Liquid phase transport properties such as viscosity and diffusivity [44, 71, 72], intermediate scattering function and dynamical structure factor [57] are also given in the fifth chapter. Hydrodynamic limit properties

6

of intermediate scattering function and dynamical structure factor are investigated and compared to static structure factor. Additionally, bulk modulus and compressibility are calculated from elastic constants and initial time, long wave limit results of intermediate scattering functions. Dynamic structure factors of Pd, Al and Pd-Al alloys are also investigated. It is seen that, dynamic structure factors have high first peaks. Some additional peaks [73] are observed in the hydrodynamic limit.

Conclusions are given in Chapter 6. Melting point estimation for both Pd and Al metals and $Pd_{0.8}Al_{0.2}$, $Pd_{0.6}Al_{0.4}$, $Pd_{0.4}Al_{0.6}$, and $Pd_{0.2}Al_{0.8}$ alloys are discussed. Experimental and simulated pair distribution functions and structure factors of Pd and Al liquid metals and metal alloys are discussed. Transport properties are analysed and compared with experimental results and other theoretical studies. Hydrodynamic limit properties of intermediate scattering function and dynamical structure factor are investigated and the small q region of the structure factor results are compared.

In Chapter 4, it is concluded that, the enthalpy of mixing for Pd-Al alloy coincides well with experimental data given by Hultgren [74] at 300 K. Both experimental and simulated enthalpies are observed to be negative, which implies that Pd-Al alloy has miscible character. Elastic constants are calculated between $0\ K - 300\ K$ temperature range and are found to fit very well for Pd metal and comparably well for Al metal compared with experimental elastic constants [75]. Densities are simulated between $0\ K - 300\ K$ temperatures and compared with experimental densities taken from Simmons [75]. It is observed that densities fit

very well to experimental results for both Pd and Al.

In Chapter 5, the melting point for Pd is simulated as $1820 \pm 5\ K$ which coincides with the experimental melting point. Melting point for Al is simulated as $520\ K$. This result deviates from the experimental result as 44.5%. Melting temperature of Pd-Al alloy for four different concentrations are calculated and compared with experimental data taken from Hultgren [74]. The difference between simulation and experimental results reduces as Pd concentration in Pd-Al alloy increases. Pair distributions are calculated and plotted together with experimental values taken from Waseda [68]. Simulation results fit very well to experimental values for Pd. Depending on the melting point difference, there are some differences with the experimental pair distribution function for Al. Similar results observed for static structure factors of Pd and Al.

Diffusion coefficients and shear viscosity are simulated in Chapter 5, and they are found to be in agreement with previously published experimental, theoretical and simulated data for Pd [44] and Al [72, 76, 77]. Intermediate scattering functions and dynamic structure factors for Pd and Al and Pd-Al alloys in five different concentrations are simulated. They agree well with the dynamic structure factor of Al calculated by Ebbsjö [77]. To the best of our knowledge, no data has been published dynamic structure factor or intermediate scattering function for Pd.

Free particle limit calculations of intermediate scattering function and dynamic structure factor implies that Pd and Al have strong self correlation. Bulk

8

modulus and compressibility are calculated both from hydrodynamic limit of intermediate scattering function and elastic constants. It is concluded that the bulk modulus and compressibility results which are calculated from simulated elastic constants show better agreement with previously published experimental and simulated data [44, 75, 77]. Hydrodynamic limit investigation of dynamic structure factor show that the additional peaks observed in the hydrodynamic limit agree with the "fast sound" modes which are discussed in detail in the paper by Anento and Padró [78].

CHAPTER 2

SIMULATION METHODS

In a physical system, the key information we would like to know is the motion of particles. Therefore, computer simulations are produced by solving the equations of motion of a many particle system under certain physical conditions.

Some of the advantages of simulation can be listed as follows:

i– A wide variety of physical properties can be "measured". For example, full information about the positions and velocities of all particles in a simulated system is obtained and any desired microscopic physical quantities are derived, such as the mean square displacements, velocity auto-correlations, and density of states. These quantities can not be measured directly in an experiment.

ii– Some extreme conditions, which is hard or expensive to create in a laboratory (e.g., very low or very high temperatures, very high pressures or very rapid cooling rates), can be realized by simulation.

iii– Input conditions are precisely under control, as a result, cause and effect between input and output data can be investigated and compared unambiguously.

The simulation method is also free from the restrictions employed in purely theoretical approaches to a problem. Firstly, theoretical approaches are always simplified as much as possible, but computer simulation approach does not need

to, because complexity of a case does not introduce a problem. Secondly, computer simulations are intended to be used to calculate the exact solutions, not the approximated results.

2.1 Molecular Dynamics

The molecular dynamics (MD) computes phase-space trajectories of molecules which individually obey Newton's laws, i.e., trajectories (r_i, v_i) are calculated by using Newton's laws. The description of a system can be expressed by Newton's equations, a Hamiltonian or a Lagrangian. MD method solves the equation of motion numerically on a computer and obtains the static or dynamic properties of the system. For this reason, it is necessary to prepare equations for numerical calculation by appropriate modifications. As a consequence of the nature of computational methods, some errors will be introduced depending on the mathematical calculation of differential operators with discrete variables and finite difference operators.

The molecular dynamics method contains two general forms: one for a system at equilibrium and another for a system away from equilibrium. For example, in the microcanonical ensemble (EVN), equilibrium molecular dynamics is typically applied to an isolated system defined by a fixed number of molecules, N, in a fixed volume, V [79]. Because the system is isolated, the total energy, E, is also constant. Thus the variables N, V and E determine the thermodynamic state.

In EVN-molecular dynamics, atomic positions $\mathbf{r^N}$ are obtained by solving

11

Newton's equation of motion:

$$\mathbf{F_i(t) = m\ddot{r}_i(t)} = -\frac{\partial \mathcal{U}(\mathbf{r^N})}{\partial \mathbf{r_i}}, \tag{2.1}$$

where $\mathbf{F_i}$ is the force on i th atom, caused by the N-1 other atoms, the dots indicate total derivatives, and m is the atomic mass. The first integration of the equation (2.1) yields the atomic momentum, and the second integration produces the atomic positions. Continuous first and second integration for N atoms produces individual atomic trajectories from which time averages of the macroscopic properties can be computed as.

$$< A > = \lim_{t \to \infty} \frac{1}{t} \int_{t_0}^{t_0+t} A(\tau)d\tau. \tag{2.2}$$

At equilibrium this average cannot depend on the initial time t_0. Since positions are obtained, the time average (2.2) represents both static properties and dynamic properties. Dynamic modeling problem can be divided into two main tasks: Developing a suitable model for the problem and applying molecular dynamics to that model. The simulation method can be investigated as two great tasks: solving the equations of motion to generate trajectories and then analyzing these trajectories to evaluate desired properties.

Non-equilibrium molecular dynamics methods, which have first appeared in the early 1970's [80, 81], are used for computing transport coefficients. In these methods an external force is applied to the system to establish the non equilibrium situation of interest, and response of the the system to the force is then determined from the simulation. Non-equilibrium molecular dynamics has been used

to obtain the shear viscosity, bulk viscosity, thermal conductivity, and diffusion coefficients [82].

MD simulation has its own computational limitations. One of the main limitations is the computer speed and storage constraints for MD simulation. Depending on the computer limitations MD simulations are usually done on systems containing 100-1000 particles, whereas calculations involving as many as 10^6 particles have been performed [83] as well. Simulations are confined to the systems of particles that interact with relatively short-range forces depending on the size limitations; that is, inter-molecular forces should be small when molecules are separated by a distance equal to half of the smallest overall dimension of the system. Because of the speed limitation, simulations are confined to studies of relatively short-lived phenomena (i.e., less than 100-1000 ps). It is necessary to satisfy the condition that the characteristic relaxation time of the phenomenon under investigation must be small enough so that one simulation generates several relaxation times.

Molecular dynamics simulation produces thousands of data during a simulation process. For example, for 100 atoms molecular dynamics simulation produces 600 values of positions and momenta in each integration step. Considering that the integration proceeds for thousands of steps, it is not easy to compute and store such a huge amount of data.

The phase-space trajectories are the first products of MD simulations. The trajectory is analyzed by appealing to kinetic theory, statistical mechanics and sampling theory. The trajectory is tested by probing constraints established by

periodic boundary conditions and by conservation principles. All together these tools form the foundation of molecular dynamics simulation.

2.2 Hamiltonian Dynamics

It is a fact that the molecular forces and positions change in time but the functional form of Newton's second law is time independent. As a consequence, we expect there is a function of positions and velocities whose value is constant in time, this function is called the Hamiltonian $\mathcal{H}$ [57]:

$$\mathcal{H}(\mathbf{r}_N, \mathbf{p}_N) = E = constant. \tag{2.3}$$

Here the momentum of molecule i is

$$\mathbf{p}_i = m\frac{d\mathbf{r}_i}{dt} \tag{2.4}$$

For an isolated system total energy can be identified by the Hamiltonian;

$$\mathcal{H}(\mathbf{r}_N, \mathbf{p}_N) = \frac{1}{2m}\sum_i \mathbf{p}_i^2 + \mathcal{U}(\mathbf{r}_N), \tag{2.5}$$

where the potential energy $\mathcal{U}$ results from intermolecular interactions. Equation of motion can be obtained in the Hamiltonian formalism as follows:

$$\frac{d\mathcal{H}}{dt} = \sum_i \frac{\partial\mathcal{H}}{\partial\mathbf{p}_i}\dot{\mathbf{p}}_i + \sum_i \frac{\partial\mathcal{H}}{\partial\mathbf{r}_i}\dot{\mathbf{r}}_i + \frac{\partial\mathcal{H}}{\partial t}. \tag{2.6}$$

Since $\mathcal{H}$ has no explicit time dependence(2.3), then the rightmost term of (2.6) vanishes and on the left term is equal to zero. So we get,

$$\frac{\partial\mathcal{H}}{\partial\mathbf{p_i}} = \frac{\mathbf{p_i}}{m} = \dot{\mathbf{r}}_i, \tag{2.7}$$

14

and

$$\frac{\partial \mathcal{H}}{\partial \mathbf{r_i}} = \frac{\partial \mathcal{U}}{\partial \mathbf{r_i}}. \tag{2.8}$$

Since each velocity is independent of others

$$\frac{\partial \mathcal{H}}{\partial \mathbf{r}_i} = -\dot{\mathbf{p}}_i. \tag{2.9}$$

For each molecule, equations (2.7) and (2.9) are Hamilton's equations of motion. These two equations represent 6N first order differential equations, equivalent to Newton's 3N second-order equations (2.1), for a system of N particles. To demonstrate this, it is enough to eliminate $\dot{\mathbf{p}}_i$ from equation (2.9):

$$\frac{\partial \mathcal{H}}{\partial \mathbf{r}_i} = -m\ddot{\mathbf{r}}_i. \tag{2.10}$$

Using (2.8) in (2.10) and comparing with Newton's second law (2.1) gives the following result:

$$\mathbf{F}_i = -\frac{\partial \mathcal{H}}{\partial \mathbf{r}_i} = -\frac{\partial \mathcal{U}}{\partial \mathbf{r}_i}. \tag{2.11}$$

This is the expression of the fact that, any conservative (non dissipative) force can be written as the negative gradient of some function $\mathcal{U}$.

The above equation emphasizes the difference between Newtonian and Hamiltonian dynamics. Motion is a response to an applied force in the Newtonian view but forces do not appear explicitly, they occur in such a way as to preserve the Hamiltonian function in the Hamiltonian view.

A summary of the assumptions used above in obtaining Hamilton's equation of motion are given as follows;

1. An isolated system considered in which if the system interacts with its surroundings, the Hamiltonian should contain additional terms. In such a case that $\mathcal{H}$ would not represent the system's total energy, which means $\mathcal{H}$ would still be conserved, but E would not.

2. The momenta and velocities are related by (2.4).

3. The Hamiltonian was not allowed to contain any explicit time dependence. Otherwise, $\mathcal{H}$ would not be a conserved quantity.

Some new parameters, e.g., constant pressure (P) or constant temperature (T) can be added to the parameters which define the degrees of freedom besides the parameters energy (E), volume (V) and number of particles (N).

2.2.1 MD Simulation at Constant Pressure and Temperature

The molecular dynamics methods discussed so far are limited to the study of systems characterized by fixed values of N, V and E (the total energy). In certain applications, it would be useful to have the temperature and pressure included among the fixed parameters of the calculation. Several schemes have been developed for this purpose, most of which have their inspiration in a paper by Andersen [58]. The work of Andersen, and a following work by Nosé [59] are based on the concepts of an "extended" system consisting of the physical system of interest and the external reservoir. The coupling to the reservoir holds the system at constant pressure or temperature (or both) by suitable modification of the equations of motion of the particles in the system of interest.

2.2.2   Microcanonical ensemble molecular dynamics

The central method in investigation and analysis of isolated system molecular dynamics trajectories is microcanonical ensemble. In this work, we consider an isolated system with the total number of molecules N, system volume V, and total energy E are constants, for a pure substance. These variables are sufficient to fix the thermodynamics state. For any dynamical quantity $F(\mathbf{r}^N, \mathbf{p}^N)$, the microcanonical ensemble average is given by the following expression [57],

$$\langle F \rangle = \frac{1}{h^{3N} N! \omega} \int d\mathbf{r}^N d\mathbf{p}^N F(\mathbf{r}^N, \mathbf{p}^N) \, \delta[E - H]. \tag{2.12}$$

2.2.3   Molecular dynamics at constant external stress (HPN ensemble)

We used HPN ensemble to thermalize and equilibrate the system. Extended Hamiltonian formalism in Molecular Dynamics was originated from the work by Andersen [58] which became the origin of the most MD simulation methods. Andersen introduced a new dynamical variable, volume, into constant pressure simulation method as a new additional degree of freedom. The change of volume is driven by a difference between an internal pressure and external pressure. The internal pressure has been expressed as the average of the kinetic energy and the virial and includes the interaction between particles. The external pressure, equilibrating the internal pressure changes, has been controlled by a piston mass parameter introduced externally. As a result, a feedback mechanism controls the pressure at a constant value. The internal pressure is controlled to fluctuate around the external pressure such as, when the internal pressure becomes larger

than external pressure, the volume expands and the internal pressure decreases. When the internal pressure becomes smaller, the volume shrinks and the internal pressure increases. This balance of microscopically determined volume-pressure relation is a natural way to realize a constant pressure condition.

Parinello and Rahman [86, 87] extended constant pressure method to include the shape changes of a basic MD unit cell. With the aid of this extension, direct simulation of structure changes in a solid are made to be possible. This extension was formulated so that the particles choose a stable condition themselves. Since only changes in the volume of MD cell were possible but not in its shape in Andersen's formalism [58], this extension define the developments on that formalism.

In this ensemble, the system still consists of N particles in a cell that is periodically repeated to fill all space, but in this ensemble the cell can have arbitrary shape and volume. $\mathbf{a}$, $\mathbf{b}$, and $\mathbf{c}$ vectors, that span the edges, completely describe the MD cell. The tree vectors $\mathbf{a}$, $\mathbf{b}$, and $\mathbf{c}$ can have different lengths and arbitrary mutual orientations. The vectors are arranged as h={$\mathbf{a}$, $\mathbf{b}$, $\mathbf{c}$} to form a 3×3 matrix. As a result the volume is given by,

$$\Omega = \|\mathbf{h}\| = \mathbf{a} \cdot (\mathbf{b} \times \mathbf{c}). \qquad (2.13)$$

In the case when only hydrostatic pressure is applied, the variability in the shape and size of MD cell was obtained by Parinello and Rahman [86] as follows: the usual set of $3N$ dynamical variables, that describe the positions of the N particles, was increased by the 9 components of $\mathbf{h}$. The time evolution of the

18

$3N + 9$ variables was then obtained from the Lagrangian [87],

$$\mathcal{L} = 1/2 \sum_{i=1}^{N} m_i \dot{\mathbf{s}}_i' \mathbf{G} \dot{\mathbf{s}}_i - \sum_{i=1}^{N} \sum_{j>i}^{N} \phi(r_{ij}) + 1/2W \ Tr[\dot{\mathbf{h}}' \dot{\mathbf{h}}] - P\Omega, \quad (2.14)$$

where P is the hydrostatic pressure that we intended to impose on the system and W is the piston mass, and $\mathbf{G}$ is the metric tensor, $\mathbf{G} = \mathbf{h}' \ \mathbf{h}$. The position $\mathbf{r}_i$ of particle i is written in terms of $\mathbf{h}$ and components ξ_i, η_i, and ζ_i as,

$$\mathbf{r_i} = \mathbf{h s_i} = \xi_\mathbf{i} \mathbf{a} + \eta_\mathbf{i} \mathbf{b} + \zeta_\mathbf{i} \mathbf{c}. \quad (2.15)$$

The Hamiltonian can be constructed from Eq. (2.14), following the usual rules of the mechanics [87]. Since the system is not subjected to time dependent external forces, the Hamiltonian can be written as;

$$\mathcal{H} = \sum_{i=1}^{N} 1/2 m_i \mathbf{v}_i^2 + \sum_{i=1}^{N} \sum_{j>i}^{N} \phi(r_{ij}) + 1/2WTr[\dot{\mathbf{h}}' \dot{\mathbf{h}}] + p\Omega. \quad (2.16)$$

In equilibrium, the constant of motion $\mathcal{H}$ gives the Enthalpy, H,

$$H = E + p\Omega, \quad (2.17)$$

where

$$E = \sum_{i=1}^{N} 1/2 m_i \mathbf{v}_i^2 + \sum_{i=1}^{N} \sum_{j>i}^{N} \phi(r_{ij}). \quad (2.18)$$

As a result, the Lagrangian in Eq. 2.14 defines a HPN dynamics. Detailed information can be extracted from related studies of Andersen [58] and Parinello [87], and Uludoğan [88].

2.2.4   Molecular dynamics at constant temperature (TPN ensemble)

TPN ensemble, which is added to MD simulation by Nosé [59, 60], is used to perform production runs in this work. Nosé introduced a new degree of freedom,

related to constant temperature, to the physical system. This freedom corresponds to a thermal reservoir and extends the Andersen [58] TVN ensemble MD method. Since the system is in contact with a thermal reservoir, energy flows dynamically from the reservoir to the system and back. The volume of sample is controlled by using a piston. The extra degree of freedom is denoted by "s" which acts as an external system. In the TPN ensemble, the virtual variables $(\mathbf{q}_i, \mathbf{p}_i, s, V, t')$ are related to the real variables $(\mathbf{q}'_i, \mathbf{p}'_i, s, V, t')$ via scaling of the coordinates by $V^{1/3}$ and scaling of time by s (V, the volume of a MD cell) [60],

$$\mathbf{q}'_i = V^{1/3}\mathbf{q}_i, \tag{2.19}$$

$$\mathbf{p}'_i = \frac{\mathbf{p}_i}{V^{1/3}s}, \tag{2.20}$$

$$t' = \int^t \frac{dt}{s}, \tag{2.21}$$

where $\mathbf{q}_i$ components are limited to the range of 0 to 1. The Hamiltonian [60] of the extended system is

$$\mathcal{H} = \sum_i \frac{\mathbf{p}_i^2}{2m_i V^{2/3}s^2} + \phi(V^{1/3}\mathbf{q}) + \frac{p_s^2}{2Q} + gkT \ ln \ s + \frac{p_v^2}{2W} + P_{ex}V, \tag{2.22}$$

where p_v is the conjugate momentum of V, W is a mass for the motion of volume, and P_{ex} is the external pressure.

For virtual time display with $g = 3N+1$, the equilibrium distribution function is

$$\rho(\mathbf{p}', \mathbf{q}', V) = \exp[-(H_0(\mathbf{p}', \mathbf{q}') + P_{ex}V)/kT], \tag{2.23}$$

20

and the averages of any function calculated from trajectories, $\mathbf{p}', \mathbf{q}', V$, are identical with those in the TPN ensemble;

$$\lim_{t_0 \to \infty} \frac{1}{t_0} \int_0^{t_0} F(\mathbf{p}/V^{1/3}s, V^{1/3}\mathbf{q}, V)dt \;=\; \langle (\mathbf{p}/V^{1/3}s, V^{1/3}\mathbf{q}, V) \rangle \quad (2.24)$$

$$=\; \langle F(\mathbf{p}', \mathbf{q}', V) \rangle$$

$$=\; F_{TPN}(N, P_{ex}, T).$$

Detailed information is given in the paper by Nosé [60].

2.2.5 Molecular Dynamics Algorithms

In most MD simulations most of the computation time is used to computing interactions, and every effort is made to ensure that this is done as efficiently as possible. Instead of a direct evaluation, interactions can be computed by using a simple method mostly accompanied by interpolation for additional accuracy.

There are number of different numerical methods for integrating the equations of motion. Most of these methods can be ignored for the simple reason that the hardest component of the computation is the force evaluation, and any integration method requiring more than one such calculation per time-step is wasteful, unless it can deliver a proportionate increase in the size of time-step Δt while maintaining the same accuracy. It is neither a realistic nor a practical goal to obtain a high degree of accuracy in the trajectories [93]. The sharply repulsive potentials result in trajectories for which even the most minute numerical errors grow exponentially with time. This is not merely a mathematical curiosity, it also corresponds to what happens in nature, and the accuracy of several average

collision times is not a meaningful issue. As a result, the criteria for choosing a numerical method relies on energy conservation and on the ability to reproduce certain time and space-dependent correlations for a sufficient degree of accuracy.

Predictor-corrector algorithms, which is one of the most well known numerical methods, e.g., Verlet algorithms or Gear's Predictor-corrector algorithms, were first used in molecular dynamics by Rahman [40, 90]. in this study, we used Gear's predictor-corrector algorithm [90, 91] which has the following steps:

a- Predict positions of atoms in crystal $\mathbf{r_i}$ at time $t + \delta t$ using a fifth-order Taylor series based on positions and their derivatives at time t. The derivatives $\dot{\mathbf{r}}_\mathbf{i}$, $\ddot{\mathbf{r}}_\mathbf{i}$, $\mathbf{r^{iii}}_\mathbf{i}$, $\mathbf{r^{iv}}_\mathbf{i}$ and $\mathbf{r^v}_\mathbf{i}$ are needed at each step. These are also predicted at time $t + \delta t$ by applying Taylor expansion at time t.

$$
\begin{aligned}
r_i(t + \delta t) &= r_i(t) + \dot{r}_i(t)\delta t + \ddot{r}_i(t)\frac{(\delta t)^2}{2!} + ... + r_i^{(v)}(t)\frac{(\delta t)^5}{5!}, \\
\dot{r}_i(t + \delta t) &= \dot{r}_i(t) + \ddot{r}_i(t)\delta t + r_i^{(iii)}(t)\frac{(\delta t)^2}{2!} + ... + r_i^{(v)}(t)\frac{(\delta t)^4}{4!}, \\
\ddot{r}_i(t + \delta t) &= \ddot{r}_i(t) + r_i^{(iii)}(t)\delta t + r_i^{(iv)}(t)\frac{(\delta t)^2}{2!} + r_i^{(v)}(t)\frac{(\delta t)^3}{3!}, \quad\quad (2.25) \\
r_i^{(iii)}(t + \delta t) &= r_i^{(iii)}(t) + r_i^{(iv)}(t)\delta t + r_i^{(v)}(t)\frac{(\delta t)^2}{2!}, \\
r_i^{(iv)}(t + \delta t) &= r_i^{(iv)}(t) + r_i^{(v)}(t)\delta t, \\
r_i^{(v)}(t + \delta t) &= r_i^{(v)}(t).
\end{aligned}
$$

b- Evaluate the inter-molecular force F_i on each molecule at time $t + \delta t$ using the predicted positions. For continuous potential energy functions $u(r_{ij})$ that acts

22

between atoms i and j, the force on each molecule is given by

$$\mathbf{F}_i = -\sum_{i \neq j} \frac{\partial u(r_{ij})}{\partial r_{ij}} \hat{\mathbf{r}}_{ij} \tag{2.26}$$

Apply Newton's third law:

$$\mathbf{F}(r_{ij}) = -\mathbf{F}(r_{ji}) \tag{2.27}$$

to decrease the amount of computation by a factor of two.

c- Correct the predicted positions and their derivatives using the discrepancy $\delta \ddot{r}_i$ between the predicted acceleration and that given by the evaluated force $\mathbf{F_i}$. With the forces at $t + \delta t$ obtained from (2.26), Newtons second law can be used to determine the accelerations $\ddot{\mathbf{r}}(\mathbf{t} + \delta \mathbf{t})$.

Hoover [82, 89], Haile [90], Allen and Tildesley [92], Rapaport [93], and Evans and Morris [94] explained the applications of equilibrium and non-equilibrium MD simulation on fluids. Some other applications are contained in the collection edited by Ciccotti and Hoover [95].

2.2.6 Periodic boundary conditions (PBC)

Depending on the memory and time restrictions, size of sample is extremely small in a simulation process. Number of atoms, N, is of order 10^3 or less in a typical study. In order to minimize surface effects and by the means of that to simulate more closely the behavior of an infinite system, it is customary to use periodic boundary conditions. The particles of interest lie in the central cell and this basic unit is surrounded on all sides by periodically repeated images of itself. Each image cell contains N particles in the same relative positions as in

23

the central cell. When a particle enters or leaves through one wall of a cell, the replacement is balanced by an image of that particle leaving or entering through the opposite wall respectively. The choice of N and the shape of the cells mostly supply advantage in such a way that the PBC generates a perfect lattice suitable to the physical system when the particles in the central cell are arranged in a proper manner. Pd and Al crystallize in a face-centered cubic structure and it is natural to use a cubic cell and take $N = 4n^3$, where n is an integer. Consequently the number of widespread use of samples contains $N = 32, 108, 256, 500, 864, ...$ particles. We used $N = 864$ particles in this study [57, 96].

2.2.7 Minimum image convention and cutoff radius

One of the most critical point of MD simulation is the calculation of the forces, acting on all molecules, and the potential energy for a particularly determined configuration. The system is thought as a sum of pairwise interactions. Pairwise interactions are calculated in particular but there are many interactions in between, such as if molecule 1 is chosen as a reference, pairwise additivity with other i molecules surrounding molecule 1 must be calculated. Then similar procedure continues for molecule 2 and so on for $N-1$ molecule. This procedure requires a large number of calculations which is practically impossible. The summation has to be restricted by making a proper approximation for a short range potential energy function to solve this problem. Consider molecule 1 to be at rest in the center of an interaction region, which has the same size and shape as the basic simulation box. The molecule will interact with all molecules whose centers lie

24

in the same region. This interaction is restricted with the closest ones of other (N-1) molecules. If the interaction region extends beyond the basic simulation box, the molecules that fall into the interaction region in neighboring boxes are included as well. This is called minimum image convention.

There are still problems with the number of calculations despite the decrease due to use of minimum image convention. The calculation of the potential energy due to pairwise additive interaction involves $\frac{1}{2}N(N-1)$ terms in the minimum image convention. This means a large number of calculations for a system of, say, 1000 particles. The problem is solved by using a cutoff radius approximation. When using cutoff radius R_C, only the neighbors inside the sphere with radius R_C concentrated on particle i contribute to the total force acting on this particle.

The cutoff radius must satisfy the condition $R_C < \frac{L}{2}$, where L is the smallest length of L_x, L_y and L_z. In the consideration of the number of particles in the cutoff region one has to make sure that every particle, interacting with i th particle is located in the simulation cell.

CHAPTER 3

INTER-ATOMIC POTENTIALS

3.1 Finnis-Sinclair potential

Pair potentials are used to describe the energy related properties of metals for many years. They were the only way to simulate defects such as dislocations, grain boundaries and cracks. Despite the absence of its theoretical foundation, the pair potential is useful for generating qualitative information, such as possible local configurations of atoms [97]. In practice, pair-potential model have some problems in the calculation of basic physical properties of matter. For example, pair potentials can not satisfy the Cauchy relation ($C_{12} = C_{44}$) in a cubic crystal [61]. Finnis and Sinclair [61] solved this problem by applying an external pressure to balance the "Cauchy pressure", $\frac{1}{2}(C_{12} - C_{44})$. This pressure is a fictitious external pressure which was produced by volume dependent term of total energy. However, the introduction of the macroscopic volume as a variable in the total energy leads to some paradox that the bulk modulus calculated by the method of long waves (constant volume) differs from its value calculated by homogeneous deformation, unless the volume-dependent term is linear in volume. This problem arises especially when the simulation of internal cavities or cracks in a metal is taken into consideration.

The pair-potential description is also inadequate in the calculation of vacancy formation energy, which is found to be nearly equal to the cohesive energy. Experimentally it is found to be about one-third of the cohesive energy [61].

Finnis-Sinclair (FS) proposed a solution to incorporate in a simple model the essential band character of metallic cohesion. The simplest expression of band structure is in the second moment-approximation to the tight-binding model (for detailed information see the Section 9 of the book by Sutton [98, 99]).

The total energy of an assembly of atoms at positions $\{\mathbf{R}_i\}$ is written as

$$U_{tot} = U_N + U_P, \tag{3.1}$$

where U_N is the N-body term and U_P is a conventional central pair-potential summation. U_N is an empirical cohesive function summed over all atoms as follows:

$$U_N = -A \sum_i f(\rho_i), \tag{3.2}$$

where

$$\rho_i = \sum_j \phi(R_{ij}), \tag{3.3}$$

$$R_{ij} = |\mathbf{R}_{ij}| = |\mathbf{R}_j - \mathbf{R}_i|, \tag{3.4}$$

and A is anticipated as a positive constant.

The main differences between the approach of Daw-Baskes and Finnis-Sinclair is the derivation and interpretation of ρ, and the embedding function f. Finnis-Sinclair chose $f(\rho)$ to be $\sqrt{\rho}$ and identified ρ with the second moment of the density of states from the tight-binding theory [100] and $\phi(R)$ was interpreted

as a sum of squares of overlap integrals [101]. Daw and Baskes specified ρ as an atomic charge density obtained from Hartree-Fock calculations for the free atom. They obtained an embedding function $f(\rho)$ by empirical fitting. Finnis-Sinclair expressed the second term of total energy of assembly of atoms as follows:

$$U_P = \frac{1}{2} \sum_{ij} V(R_{ij}). \tag{3.5}$$

U_N represents the band energy (bonding energy) and U_P is a repulsive core-core interaction in the Finnis-Sinclair tight-binding interpretation.

Finnis and Sinclair parametrized the functions ϕ and V by fitting to cohesive energy, equilibrium volume and all three elastic moduli for the bcc transition metal.

Finnis and Sinclair adopt for the cohesive energy ϕ a parabolic form,

$$\phi(R) = \begin{cases} (R-d)^2, & R \leq d, \\ 0, & R > d. \end{cases} \tag{3.6}$$

The range d is a disposable parameter which is assumed to lie between the second and third neighbors, thus

$$a < d < \sqrt{2}a,$$

where a is the lattice constant.

The pair-potential defined by Finnis and Sinclair in the quadratic polynomial is,

$$V(R) = \begin{cases} (R-c)^2(c_0 + c_1 R + c_2 R^2), & R \leq c, \\ 0, & R > c. \end{cases} \tag{3.7}$$

c is assumed to lie between second and third neighbors. c_0, c_1 and c_2 are the parameters free for fitting experimental data. To ease the fitting conditions Finnis and Sinclair considered that all the physical quantities are linear in c_0, c_1 and c_2, in addition to a.

3.1.1 Sutton-Chen (SC) potential

In this study, Sutton-Chen potential [62] with Quantum Sutton-Chen potential parameters [64, 65, 66] is used for pure metal simulations. Sutton and Chen interested in long-range Finnis-Sinclair empirical potentials to perform better computer simulations. They modeled the mechanical interactions between clusters of atoms. Pethica and Sutton [102] have already modeled interactions between clusters of atoms by using Lennard-Jones pair potential and they stated that there exists a mechanical instability when two slabs of material are brought into contact. They discovered that interaction between slabs is critically dependent on the range of the potential. Pethica and Sutton have chosen the Lennard-Jones pair potential because the potential correctly described the long-range van der Waals interactions between the slabs. This is not seen performable by using Finnis-Sinclair potential, which extends typically up to third neighbors in fcc and bcc crystals and does not have a $1/r^6$ van der Waals tail. Nevertheless, Lennard-Jones potential gives poor description of surface relaxation in metals. Sutton and Chen developed the Finnis-Sinclair potential with along-range interaction.

$$E_{tot} = \sum_i \left[\frac{1}{2} \sum_{j \neq j} \varepsilon_{ij} V\left(r_{ij}\right) - c_i \sum_i \varepsilon_{ii} \sqrt{\rho_i} \right], \tag{3.8}$$

29

where

$$V\left(r_{ij}\right) = \left(\frac{\alpha_{ij}}{r_{ij}}\right)^{n_{ij}}, \tag{3.9}$$

and

$$\rho_i = \sum_{i \neq j} \left(\frac{\alpha_{ij}}{r_{ij}}\right)^{m_{ij}}. \tag{3.10}$$

Here $V(r)$ is a pair potential accounting for repulsion between the i and j atomic cores and ρ_i is a local density accounting for cohesion associated with atom i. r_{ij} is the distance between atoms i and j, α is a length scaling parameter (leading to dimensionless V and ρ), c is a dimensionless parameter scaling attractive terms, ε sets the overall energy scale, and n and m are integer parameters such that $n > m$ satisfying the elastic stability conditions.

The combination rules for alloys are given by the following relations.

$$
\begin{align}
m_{ij} &= \frac{1}{2}\left(m_i + m_j\right), \\
n^{ij} &= \frac{1}{2}\left(n_i + n_j\right), \\
a_{ij} &= \frac{1}{2}\left(a^i + a^j\right), \\
\varepsilon_{ij} &= \left(\varepsilon^i \varepsilon^j\right)^{\frac{1}{2}}. \tag{3.11}
\end{align}
$$

The exponents (n, m), c are determined by the element of central atom i and j at equilibrium for each component of alloy. ε_{ij} is determined by the total cohesive energy $(E_{coh.})$ for each component of alloy. Sutton and Chen restricted m to be greater than 6.

3.1.2 Rafii-Tabar and Sutton development for fcc binary metal alloys

The Rafii-Tabar and Sutton [63] introduced a new formalism for alloy simulations. They extended Sutton-Chen potential for fcc binary metal alloys by constructing long-range Finnis-Sinclair type potential. They modeled both long- and short-range atomic interactions between unlike metallic species. They did not fit any new parameters for the alloy potential but instead they used a set parametrization rules. They generalized Eq. 3.9 and Eq. 3.10 to describe binary A-B alloys by expressing the Hamiltonian in the following Finnis-Sinclair form.

$$
\begin{aligned}
\mathcal{H} = \frac{1}{2} & \left[\sum \sum_{i \neq j} \hat{p}_i \hat{p}_j V^{AA}(r_{ij}) + (1-\hat{p}_i)(1-\hat{p}_j) V^{BB}(r_{ij}) \right. \\
& \left. + [\hat{p}_i(1-\hat{p}_j) + \hat{p}_j(1-\hat{p}_i)] V^{BB}(r_{ij}) \right] \\
& - d^{AA} \sum_i \hat{p}_i \left[\sum_{i \neq j} \hat{p}_j \phi^{AA}(r_{ij}) + (1-\hat{p}_j)\phi^{AB}(r_{ij}) \right]^{\frac{1}{2}} \\
& - d^{BB} \sum_i (1-\hat{p}_i) \left[\sum_{i \neq j} (1-\hat{p}_j)\phi^{BB}(r_{ij}) + \hat{p}_j \phi^{AB}(r_{ij}) \right]^{\frac{1}{2}}, \quad (3.12)
\end{aligned}
$$

where $\hat{p}_i$ is the site occupancy term which is defined as follows:

$$
\hat{p}_i = \begin{cases} 1, & \text{if site } i \text{ is occupied by an A atom,} \\ 0, & \text{if site } i \text{ is occupied by an B atom.} \end{cases} \quad (3.13)
$$

V^{AA}, V^{BB}, V^{AB}, ϕ^{AA}, ϕ^{BB} and ϕ^{AB} functions are defined as follows:

$$
V^{AA}(r) = \varepsilon^{AA} \left[\frac{a^{AA}}{r} \right]^{n^{AA}} \quad etc., \quad (3.14)
$$

$$
\phi^{AA}(r) = \left[\frac{a^{AA}}{r} \right]^{m^{AA}} \quad etc., \quad (3.15)
$$

The constants d^{AA} and d^{BB} are defined as;

$$
d^{AA} = \varepsilon^{AA} c^{AA} \quad \text{and} \quad d^{BB} = \varepsilon^{BB} c^{BB}, \quad (3.16)
$$

where ε^{AA}, c^{AA}, a^{AA} m^{AA} and n^{AA} are equivalent to the parameters ε, c, α, m

and n parameters of pure A metal as seen in Eqs. 3.8-3.10. Similar procedure is

valid for ε^{BB}, c^{BB}, a^{BB} m^{BB} and n^{BB} and ε, c, α, m and n parameters of pure

B metal but the other four parameters, ε^{AB}, a^{AB} m^{AB} and n^{AB}, remain to be

determined. Assuming that the functions V^{AB} and ϕ^{AB} may be expressed as;

$$V^{AB} = (V^{AA}V^{BB})^{\frac{1}{2}} \quad \text{and} \quad \phi^{AB} = (\phi^{AA}\phi^{BB})^{\frac{1}{2}}, \tag{3.17}$$

Rafii-Tabar and Sutton changed the lattice parameter, a, combination rule of SC

form as,

$$a^{AB} = \left(a^{AA} + a^{BB}\right)^{\frac{1}{2}}. \tag{3.18}$$

3.1.3 Quantum Sutton-Chen parametrization (Q-SC)

The empirical many-body force fields (FF) of the SC type used in this study

are re-parametrized by Kimura *et al.*[64, 65] for the fcc metals, by fitting to exper-

imental properties such as density, cohesive energy, moduli and phonon frequen-

cies including the zero-point energy effects, and named as Quantum Sutton-Chen

parametrization (Q-SC). The parameters for the metals studied in this work are

listed in the Table 3.1.

SC potential is based only on the experimental lattice parameter, cohesive

energy and bulk modulus [104]. Kimura *et al.* studied the properties involv-

ing defects, surfaces, and interfaces which are not adequately described by the

SC potential with the original parametrization. They introduced the quantum

corrections to take into account zero-point energy. This gives the potential the

ability of better calculation of temperature dependent properties of crystals. The phonon frequencies (at the X point), vacancy formation energies, and surface energies have been taken into account in this formalism [64, 65]. These additional values produced more powerful parametrization for SC potential, especially in the defect, surface and elastic properties.

Sutton and Chen restricted m to be greater than 6 and used the integral power indices giving the closest agreement with the bulk modulus (B) and elastic constants.

Kimura *et al.* studied the ε, c, n and m parameters of SC potential, given by Eq. (3.8) in Section 3.1.1. Relaxing the condition that n and m be integral, the B and the Cauchy discrepancy or pressure $(P_c = C_{12} - C_{44})$ can be exactly fit to the following analytical solutions;

$$n = \sqrt[3]{\left(\frac{\Omega B}{E_{coh.}}\right)\left(\frac{B}{2P_c} + 1\right)},$$

$$m = \sqrt[6]{\frac{\left(\frac{\Omega B}{E_{coh.}}\right)}{\left(\frac{B}{2P_c} + 1\right)}}, \tag{3.19}$$

where Ω is the volume per atom.

Kimura and colleagues proceed through the following steps to determine the ε, c, n and m parameters of the SC potential [64]:

i− a was set to be the experimental lattice parameter at $0K$ (Sutton and Chen set a as the lattice parameter at room temperature). The parameter c is chosen to obtain $U_{tot} = -E_{coh.}$, where $E_{coh.}$ is the experimental cohesive energy at $0K$.

ii− Bulk modulus (B) and elastic constants (c_{11}, c_{12}, c_{44}) at $0K$ are fit to experimental values.

iii$-$ Phonon frequencies $(\omega_x^T \omega_x^L)$ at the point X in the Brillouin zone are fitted by using experimental lattice spacing at room temperature to calculate the phonon dispersion curves.

iv$-$ Previous steps were carried out for a wide range of the exponents (n, m), and several candidate sets were selected that lead to good agreement between calculation and experiment.

v$-$ For each set of (c, ε, n, m) from step iv, vacancy formation energy, surface energy and equation of state were evaluated and final properties agree best when these parameters were selected.

vi$-$ The parameter a is chosen as the experimental lattice parameter at $0K$.

vii$-$ The phonon modes were calculated at the lattice parameters for $0K$ and total zero point energy obtained by summing over the brillouin zone. Parameters c and ε were optimized so that

$$F_{0K} = -E_{coh.}, \tag{3.20}$$

simultaneously with the quantum zero-pressure equilibrium conditions;

viii$-$ The phonon dispersion curve were calculated by using the room temperature lattice parameter to compare with experiment as in step **iii**.

ix$-$ Vacancy formation energy, surface energy, equation of state, thermal expansion, and specific heat as a function of temperature were calculated by using the phonon correction from previous last step.

x$-$ The best set, predicting the properties, of parameters were chosen. Table. 3.1 represents the Q-SC parameters for Pd and Al metals.

Table 3.1: Parameters for Q-SC force-field [64, 65]

metal	n	m	$\epsilon(eV)$	c	α
Pd	12	6	3.2864E-3	148.205	3.8813
Al	7	6	3.3307E-3	16.4600	4.0490

3.1.4 Details of Simulation

In this study, the borders of the simulation box extends up to sixth nearest neighbor atom. Thus a cubic system consists of 864 atoms randomly distributed on a fcc lattice. In the HPN (constant enthalpy-constant pressure) runs, the system is slowly heated from 0.1K to the target temperature by 1K/step. This procedure is followed by equilibrium (strict velocity scaling) runs which are 5000 steps. Here the temperature is constant for every target temperature. TPN type of runs are based on the equilibrium runs of HPN ones. TPN runs are constructed as 20000 steps in this study and the aim is to calculate the volume, density and enthalpy of system for each concentration. The resulting zero strain average matrix $< h_0 >$ is used in calculating pressure dependent properties of the system over 50000 steps of EVN dynamics. Fifth order Gear predictor-corrector algorithm is used in $\Delta t = 0.0020$ ps interval. Parinello-Rahman piston mass parameter is chosen as W=400 and for TPN runs the Nosé-Hoover parameter is set to Q=100.

CHAPTER 4

SOLID STATE PROPERTIES

Although dynamical properties of liquid metal and alloys are studied in this work, it is also found necessary to investigate some crucial solid properties of Pd and Al, Pd-Al alloys, because Q-SC potential parameters have been fit to 0K properties of fcc metals. Q-SC simulation results are compared with available experimental data to show the validity of Q-SC parameters for these given metals. Unfortunately, we could not find any experimental data for high temperatures to compare with our findings.

4.1   Enthalpy of mixing

Enthalpy of mixing gives information about the miscibility of two different species and it is of great interest. Hultgren[74] performed calorimetric experiments and determined the enthalpy of mixing, ΔH. Q-SC potential gives reasonable results for enthalpy of mixing when applied to Pd-Al alloy system as seen in Fig. 4.1. Q-SC simulation and experimental results [74] both have same negative sign at T= 300 K. These results imply that Pd and Al have high miscibility. On the other hand, the difference between the sizes of Pd and Al supports these results.

Although both Q-SC simulation and experimental results seem to agree well,
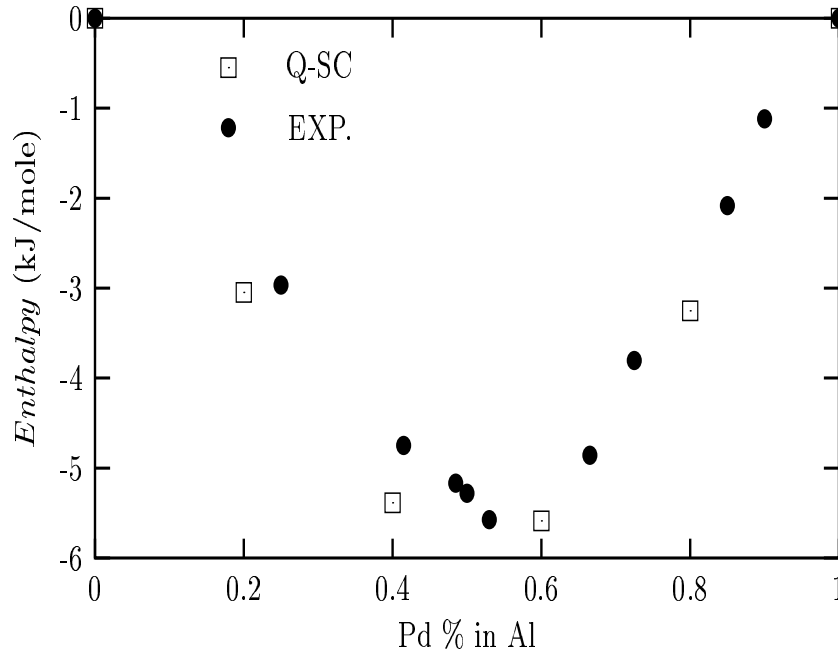
Figure 4.1: Enthalpy of mixing for Pd-Al alloys produced by TPN-MD simulation and Q-SC potential parameters at 300 K

.

there are also some differences. These differences mostly originate from potential parameters and combination rules. The parameters were fitted to pure metals but it is not exactly known whether these parameters define the alloy behavior of Pd and Al.

4.2 Elastic constants

We produced elastic constants as a result of EVN MD simulation. Comparison between experimental and calculated elastic constants shows that Q-SC potential produces very satisfactory results for Pd and Al. Elastic constants are the components of bulk modulus $B = \frac{1}{3}(c_{11} + 2c_{12})$ [75]. Fig. 4.2, Fig. 4.3 and Fig. 4.4 illustrate the elastic constants for Pd and Al.

Fig. 4.2 and Fig. 4.3 include c_{11} and c_{44} elastic constants and Fig. 4.4 includes

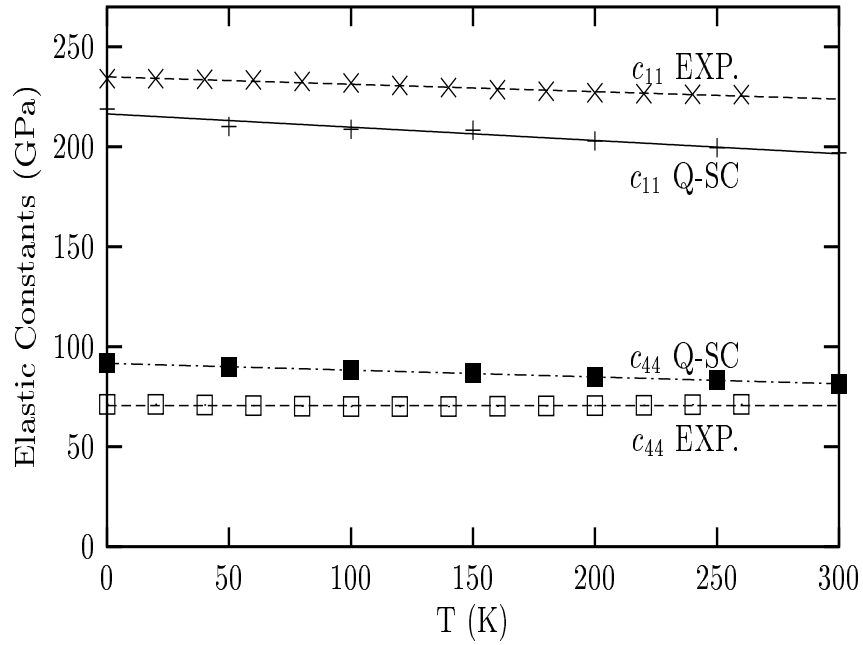Figure 4.2: Experimental and simulated elastic constants for Pd produced by EVN-MD simulation and Q-SC potential.
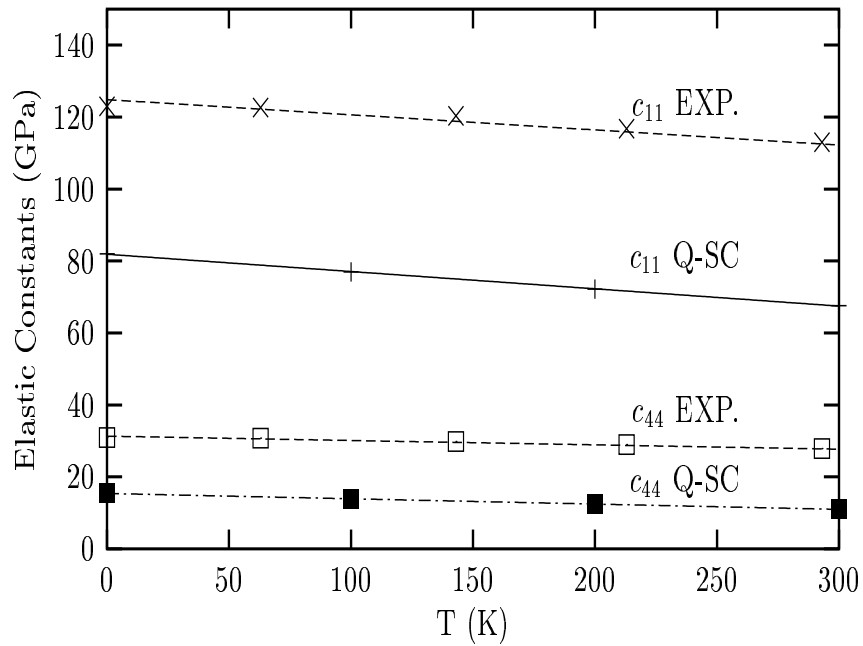
Figure 4.3: Experimental and simulated elastic constants for Al produced by EVN-MD simulation and Q-SC potential.
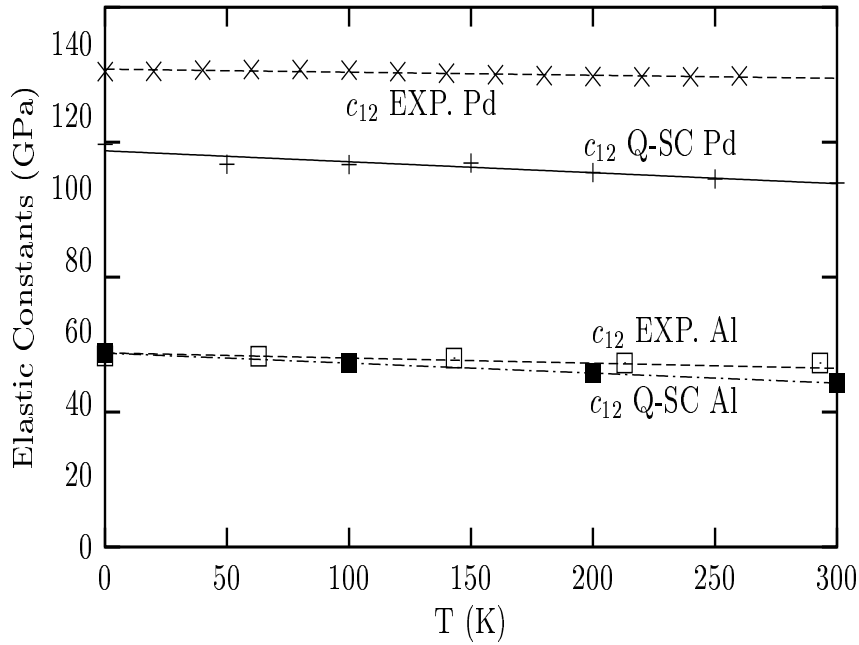
Figure 4.4: Experimental and simulated elastic constants for Pd and Al produced by EVN-MD simulation and Q-SC potential.

c_{12} elastic constants for both Pd and Al. Experimental and calculated values have some differences, but these differences are in acceptable limits (about 5% for Pd and 10-15% for Al metals in c_{11} and c_{44} elastic constants). c_{12} elastic constants for Al fit very well.

4.3 Density

The correct simulation of density has a great importance for computer simulation results. Simulation of density is also important for the investigation of scientific and industrial properties of material. Q-SC potential is very satisfactory at the density simulation for solid state densities of Pd and Al. Table 4.1 and 4.2 show the experimental and simulated densities of Pd and Al, respectively at relavant temperatures, experimental data are taken from Simmons [75].

Table 4.1: Experimental and simulated densities of Pd with respect to temperature.

T (K)	EXP. ρ (g/cm^3)	Q-SC
0	12.0690	12.1560
50	12.0675	12.1251
100	12.0650	12.0916
160	12.0569	12.0578
200	12.0515	12.0238
260	12.0434	11.9893

Table 4.2: Experimental and simulated densities of Al with respect to temperature.

T (K)	EXP. ρ (g/cm^3)	Q-SC
0	2.7333	2.6992
63	2.7311	2.6840
100		2.6648
143	2.7233	2.6435
200		2.6288
213	2.7105	2.6275
293	2.6976	2.6189
300		2.5903

CHAPTER 5

DYNAMICAL PROPERTIES

5.1   Introduction

Because complete trajectories are available, it is not difficult to measure time-
dependent properties, both in and out of equilibrium. It is not difficult to measure
thermodynamic and structural properties, such as pair distribution function and
structure factor at equilibrium. Here, we also concentrate on properties defined
in terms of time-dependent correlation functions at the atomic level, the dynamic
structure factor, and transport coefficients such as diffusion and the shear viscos-
ity.

5.2   Melting Points

When simulations are performed at points near the melting curve or whenever
a simulation is started from a lattice structure, there is an interest whether the
system has melted or not. Melting temperatures are determined from the con-
tinuity in mean square displacement, discontinuity in enthalpy, and magnitude
change in diffusion coefficient, D, which increases gradually for liquids. The re-
gion during the heating process where all of these three physical properties are
satisfied together is accepted as the melting point of a material. The continuity

41

in mean square displacement is shown in the Fig. 5.1 and Fig. 5.2 for Pd and Al
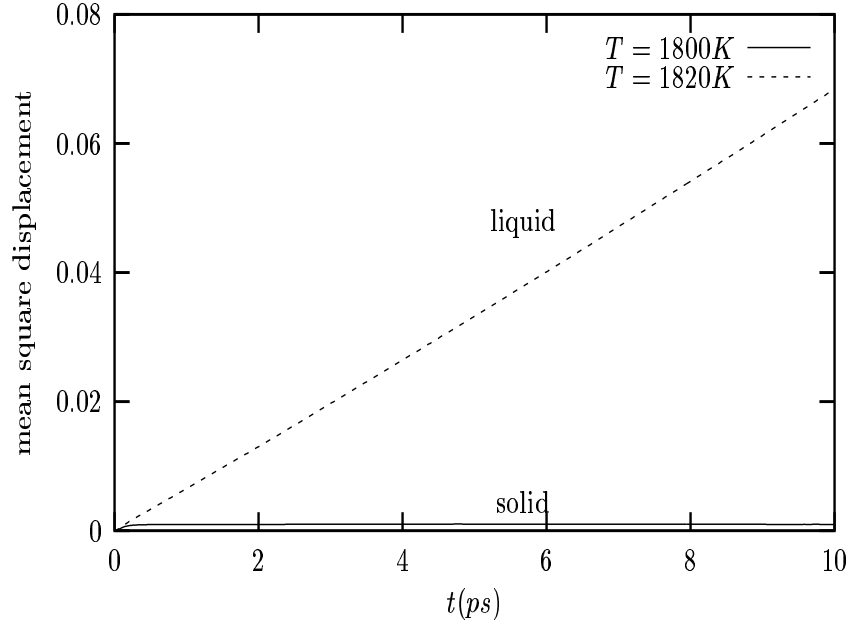
metals, respectively.

Figure 5.1: Positional mean square displacement of Pd about simulated melting point. The upper line represents the liquid state at $T = 1820K$ while the lower line represents the solid state at $T = 1800K$.

TPN MD method is used to calculate the continuity in mean square dis-

placement. On the other hand, enthalpy is calculated from EVN MD method.

Enthalpy of a system, H, carries information about the melting region. H-T

graph has a linear-like shape but it changes between the solid and liquid states.

The slight difference between the solid and liquid state values of H-T graph is

apparent in Fig. 5.3. Enthalpy of a system shows the melting point in ± 5 % error

region.

The melting points of Pd-Al alloys are calculated by using the formalism

stated by Rafii-Tabar and Sutton [63]. Rafii-Tabar and Sutton [63] modified

the potential for alloy case, but they did not perform a new parametrization for
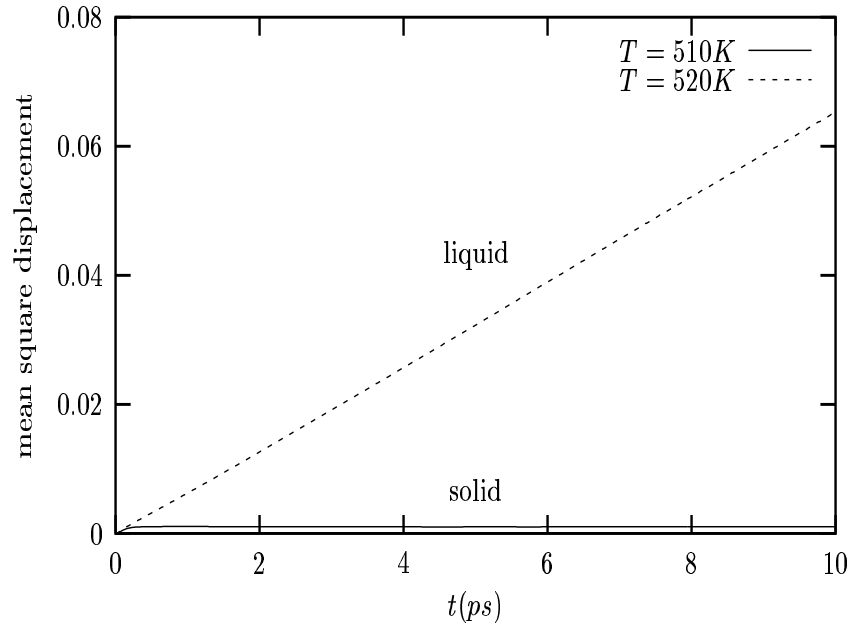
Figure 5.2: Positional mean square displacement of Al about simulated melting point. The upper line represents the liquid state at $T = 520K$ while the lower line represents the solid state at $T = 510K$.

alloys. in this work, we used the parameters produced for pure metals by Kimura *et al.* [64, 65]. The calculated and experimental melting points of Pd and Al and Pd-Al alloys in four different concentrations are given in the Table 5.1 and Fig. 5.4. Experimental melting points are predicted from Pd-Al phase diagram given in the book by Hultgren [74].

The determination of melting point is one of the challenges of MD simulation. The melting point of Al is found to be about 400 K lower than the experimental melting point of Al. But, on the other hand, the melting point of Pd is found to have nearly the same melting point as published experimental results [1]. The difference of experimental and simulated melting points is not an obstacle to study the dynamic properties of Al. On the other hand, the agreement of experimental and simulated melting points for Pd is a great success.
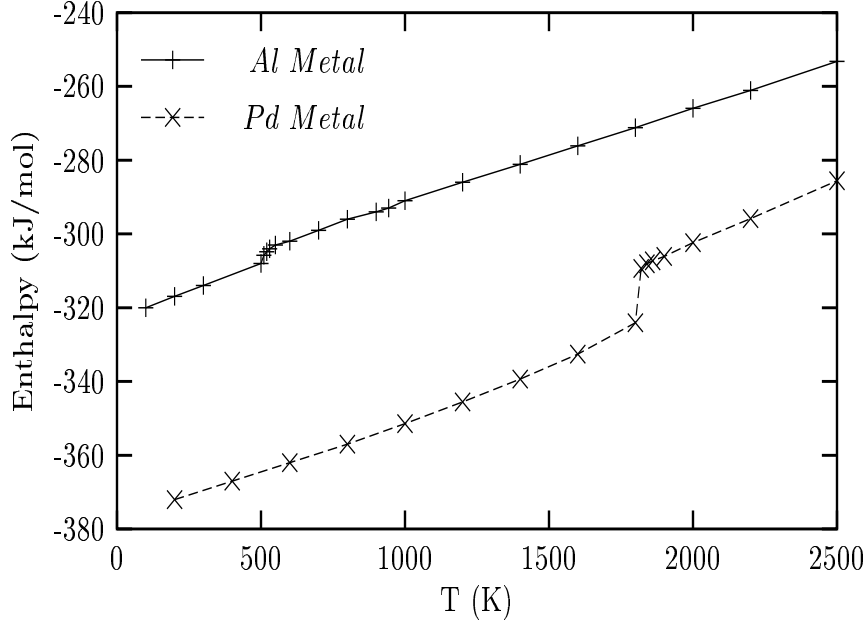
43

Figure 5.3: Enthalpy of Pd and Al with respect to temperature. The upper line represents the enthalpy of Al while the lower line represents the enthalpy of Pd.

5.3 Pair distribution function

Pair distribution function, $g(r)$, is the probability of finding another atom at a distance r from the atom at the origin $(r = 0)$ and it supplies an essential knowledge in the liquid state investigations. Pair distribution function is calculated directly from position trajectories produced by simulation. It is given by the following expression;

$$g(r) = \rho^{-2} \left\langle \sum_i \sum_{j \neq i} \delta(\mathbf{r}_i) \delta(\mathbf{r}_j - \mathbf{r}) \right\rangle = \frac{V}{N^2} \left\langle \sum_i \sum_{j \neq i} \delta(\mathbf{r} - \mathbf{r}_{ij}) \right\rangle. \qquad (5.1)$$

The experimental data is available for pure metals but not available for alloy case. Fig. 5.5 and Fig. 5.6 show the experimental (experimental values are taken from the book by Waseda [68]) and simulated $g(r)$ functions of Pd and Al at $1853K$ and at $943K$, respectively.
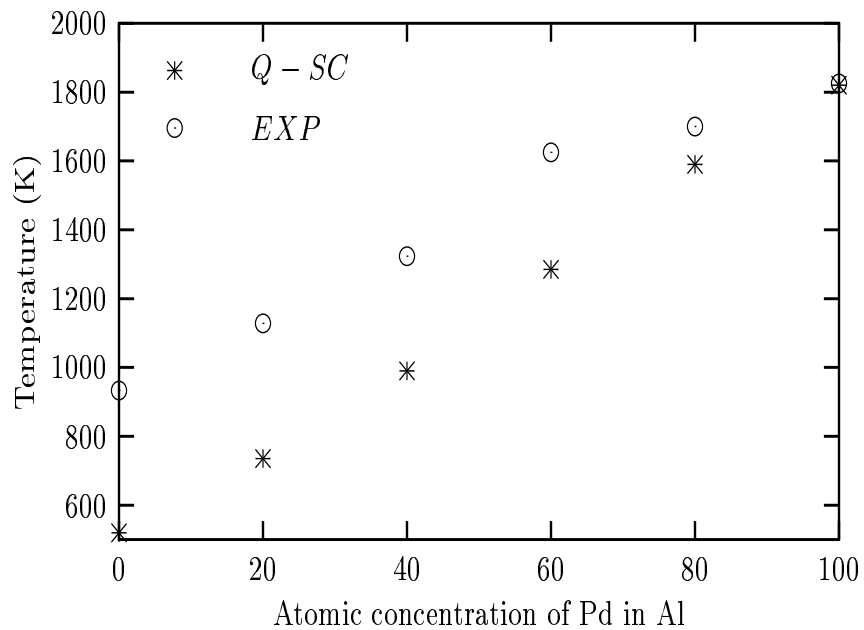
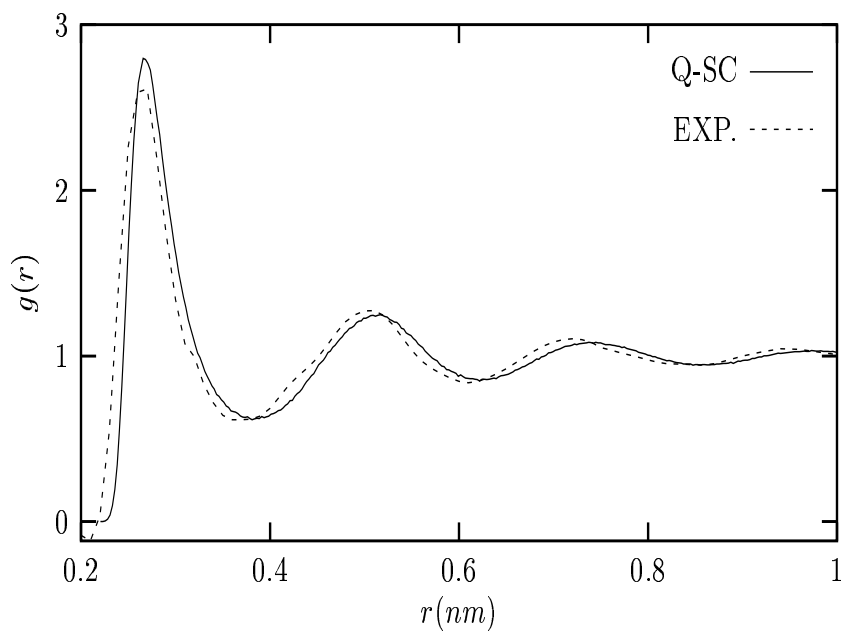Figure 5.4: Experimental and simulated melting points for Pd and Al and Pd-Al alloys in four different concentrations.

Figure 5.5: Experimental and simulated pair distribution functions for Pd ($T = 1853\ K$).

45

Table 5.1: The melting temperatures of Pd-Al alloy calculated by SC potential and Q-SC potential parameters as a function of Pd concentration in Al. Experimental data is taken from Hultgren [74].

Concentration of Pd in Al	T(K) Experiment	T(K) Simulation (Q-SC)
0.00	933	520 ± 5
0.20	1128	735 ± 5
0.40	1323	990 ± 5
0.60	1625	1285 ± 5
0.80	1700	1590 ± 5
1.00	1825	1820 ± 5

As it is seen in Fig. 5.5, simulated pair distribution function for Pd is in good agreement with the experimental data [68] and the position of first peak agrees well with the lattice parameter a for Pd. Unfortunately, it is not possible to say the same for simulated and experimental [68] pair distribution functions for Al in Fig. 5.6, because the simulated melting point is lower. The position of first peak agrees with the experimental first peak of Al. The normalized pair distribution functions of $Pd_{0.8}Al_{0.2}$ and $Pd_{0.2}Al_{0.8}$ are given in Fig. 5.7 and Fig. 5.8 at $T = 1700\ K$ and $T = 1100\ K$, respectively.

Solid, liquid and sub-melted (amorphous) phases are illustrated by the pair distribution functions, $g(\mathbf{r})$, of Pd and Al in Fig. 5.9 and Fig. 5.10 respectively. Apparent differences are observed between liquid, solid and amorphous state $g(\mathbf{r})$ functions.
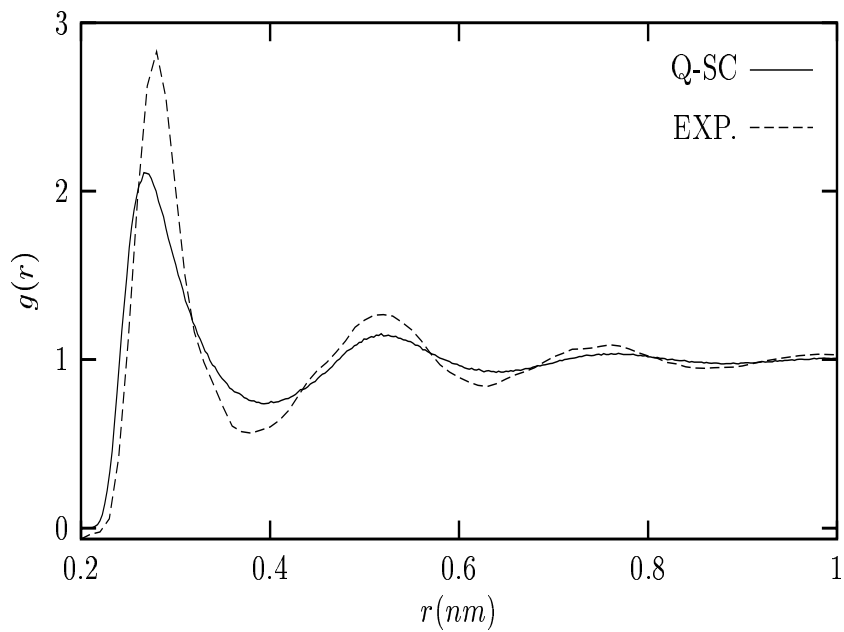
Figure 5.6: Experimental and simulated pair distribution functions for Al ($T = 943\ K$).

Figure 5.7: Simulated pair distribution functions for $Pd_{0.8}Al_{0.2}$ alloy ($T = 1700\ K$).
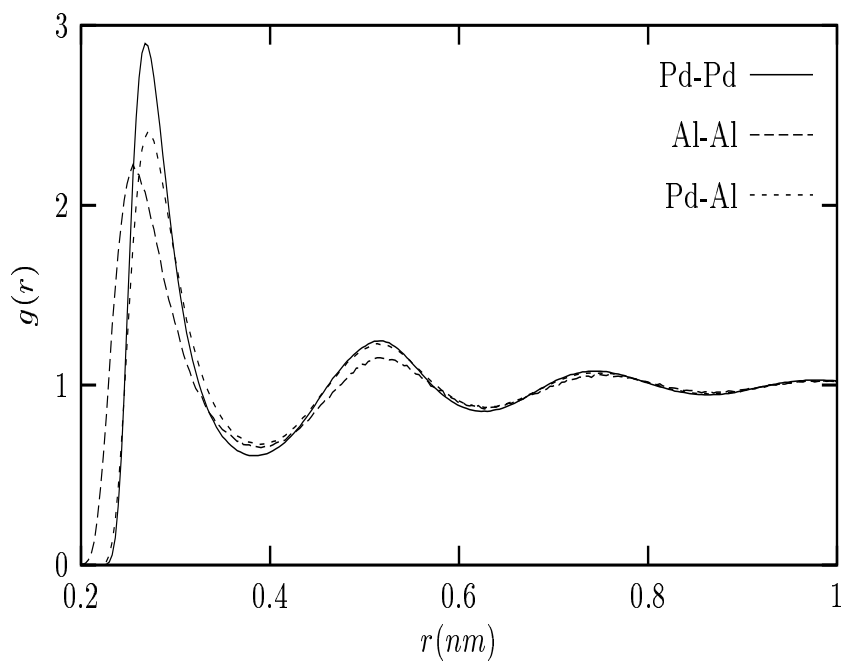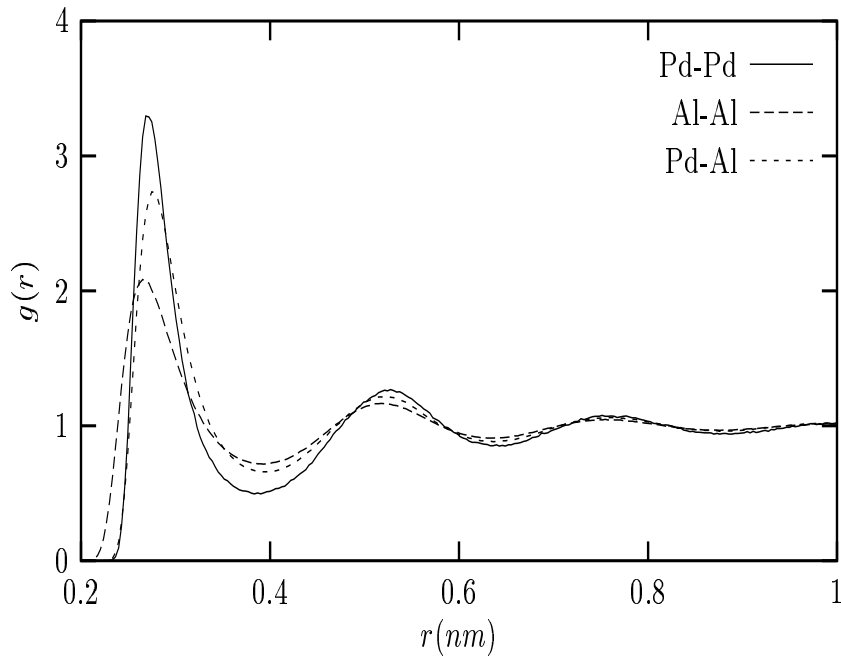
Figure 5.8: Simulated pair distribution functions for $Pd_{0.2}Al_{0.8}$ alloy ($T = 1100\ K$).

Figure 5.9: Pair distribution function of Pd in solid, liquid and sub-melted states. Solid line displays solid phase at $T = 1600K$, dashed line displays sub-melted phase (amorphous phase) at $T = 1800K$, and dotted line displays the liquid phase at $T = 1820K$.
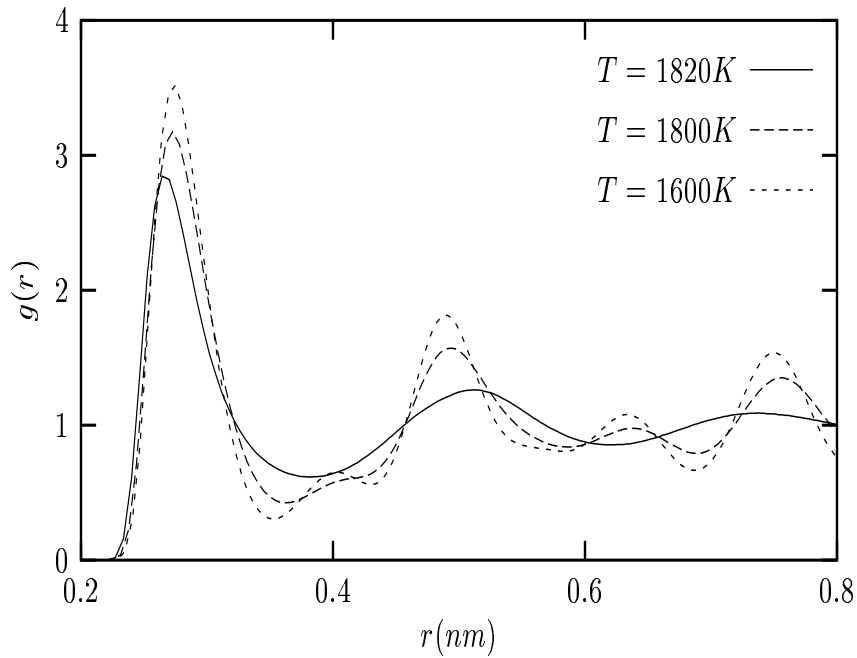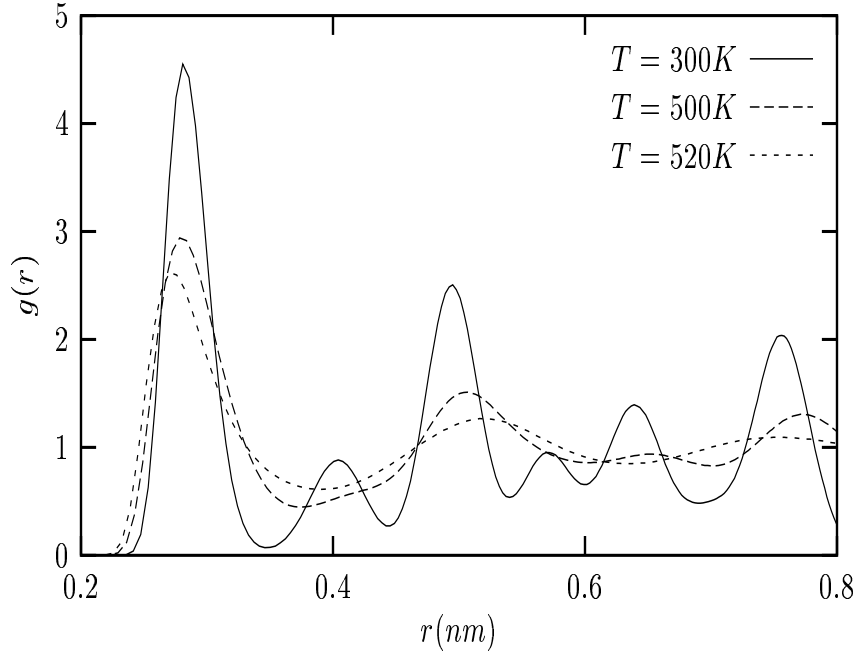
Figure 5.10: Pair distribution function of Al in solid, liquid and sub-melted states. Solid line displays solid phase at $T = 300K$, dashed line displays sub-melted phase (amorphous phase) at $T = 510K$, and dotted line displays the liquid phase at $T = 520K$.

5.4 Static Structure factor

Pair distribution is related to the structure factor $S(\mathbf{q})$ by the well known Fourier transformation of $g(\mathbf{r})$ [57, 69, 92]:

$$S(q) = 1 + 4\pi\rho \int_0^\infty r \, \frac{\sin(qr)}{q}[g(r) - 1]dr. \tag{5.2}$$

where $q = |\mathbf{q}|$ and $r = |\mathbf{r}|$. Static structure factor, $S(q)$, is an important quantity because: (a) experimental scattering profiles of liquids are system-oriented functions of $S(q)$, (b) key length-scales in liquid systems are easier to investigate from $S(q)$ than that from $g(r)$ and many analytic properties and transport coefficients are conveniently represented as functions of $S(q)$ rather than $g(r)$. Fig. 5.11 and Fig. 5.12 displays the simulated and experimental $S(q)$ values taken
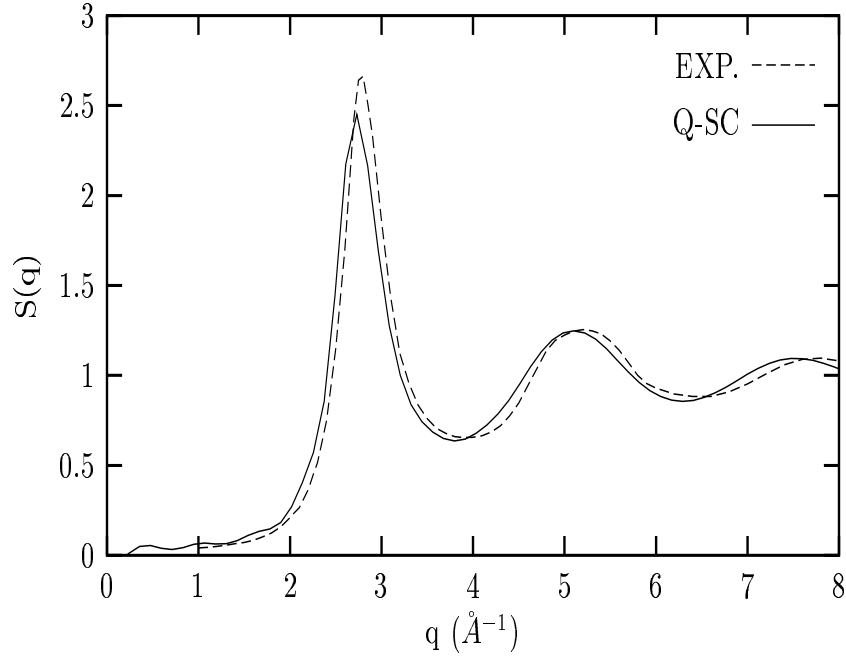
Figure 5.11: Experimental and simulated static structure factor for Pd at $T = 1853\ K$.

from Waseda [68] at $T = 1853\ K$ and $T = 943\ K$ respectively.

Fig. 5.11 displays the static structure factor of Pd. Experimental results are taken from Waseda [68]. Compared to experiment, Q-SC $S(q)$ results fit to experimental $S(q)$ very well. In Fig. 5.12, such agreement is not observed for Al. Fig. 5.13 and Fig. 5.14 illustrate the static structure factor of $Pd_{0.8}Al_{0.2}$ liquid alloy at $T = 1700\ K$ and the static structure factor of $Pd_{0.2}Al_{0.8}$ alloy at $T = 1100\ K$, respectively. To the best of our knowledge, there is no published experimental data for Pd-Al alloy to compare with our findings.

Since the normalization factor for distinct species, Pd-Al, is zero in Eq. (5.2), $S(q)$ oscillates around zero, but $S(q)$ oscillates around one for self species, Pd-Pd or Al-Al, in Fig. 5.13 and Fig. 5.14, respectively. Pd-Pd correlations are stronger than Al-Al correlations, but Pd-Al correlations are the strongest in Fig. 5.13.

Table 5.2: Experimental and simulated structure factor values of Pd at the extremum points of $S(q)$.

$T = 1853\ (K)$		
q ($\mathring{A}^{-1}$)	$S(q)$ $Q - SC$	$S(q)$ $EXP.$
1.00	0.041	0.067
2.80	2.662	2.451
3.90	0.654	0.646
5.20	1.255	1.236
6.40	0.883	0.878
7.80	1.096	1.083
7.80	0.952	0.951
9.00	0.952	0.951

Table 5.3: Experimental and simulated structure factor values of Al at the extremum points of $S(q)$.

$T = 943(K)$			$T = 1323\ (K)$		
q ($\mathring{A}^{-1}$)	$S(q)$ $Q - SC$	$S(q)$ $EXP.$	q ($\mathring{A}^{-1}$)	$S(q)$ $Q - SC$	$S(q)$ $EXP.$
0.450	0.0234	3.7234	1.00	0.051	0.123
2.70	2.475	1.9108	2.70	1.934	1.649
3.70	0.559	0.760	3.70	0.729	0.831
4.90	1.286	1.114	5.00	1.178	1.106
6.20	0.851	0.929	6.20	0.940	0.963
7.40	1.093	1.03	7.40	1.032	1.019
8.40	0.940	0.995	8.60	0.980	0.994
9.60	1.036	0.995	9.60	1.017	0.997
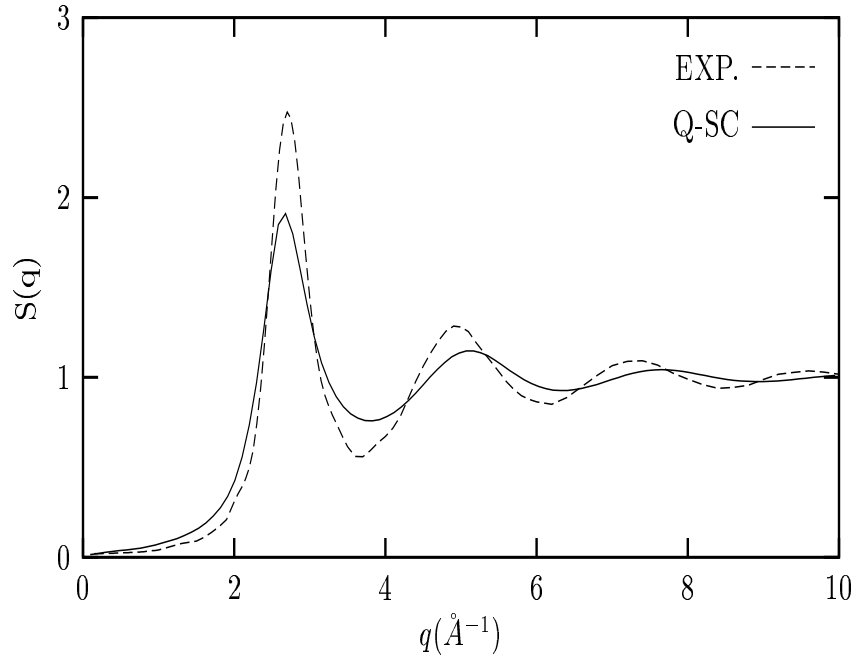
Figure 5.12: Experimental and simulated static structure factor for Al at $T = 943\ K$.

Table 5.2 and Table 5.3 are selected from the extrema of Fig.5.11 and Fig. 5.12, respectively, for a comparison between Q-SC MD simulation and experiment. As it is seen from Table 5.2 the $S(q)$ data obtained from simulated $g(r)$ data by Fourier transform agrees well with experimental $S(q)$ for Pd. But depending on the pair distribution function, we can not say the same about $S(q)$ for Al as can be seen in Table 5.3.

5.5 Diffusion Coefficients

Transport coefficients describe the material properties of a fluid in terms of fluid dynamics. Fluid dynamics is a continuum framework medium, so discrete atoms play no role in the continuum picture, but this does not limit the range of
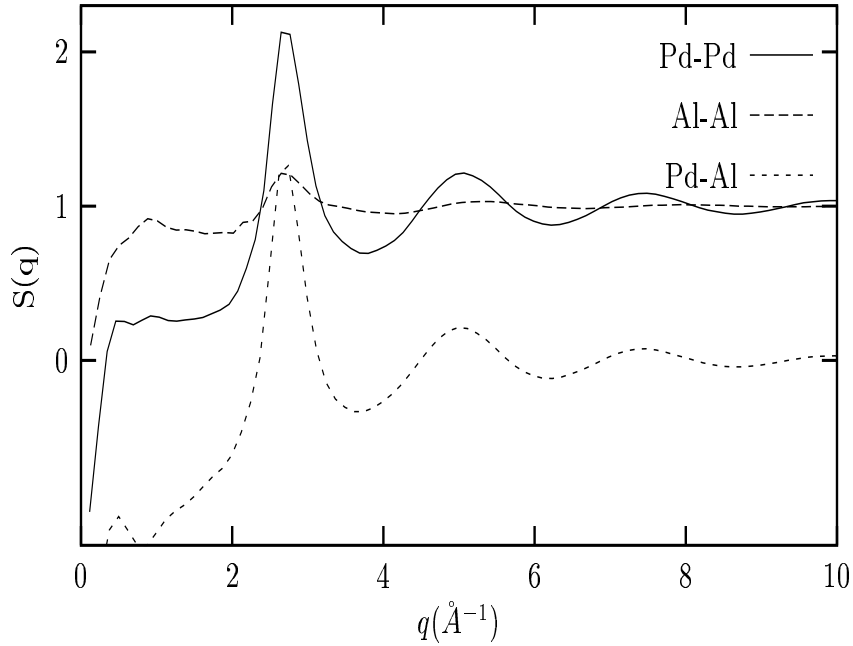
Figure 5.13: Simulated static structure factor of $Pd_{0.8}Al_{0.2}$ liquid alloy at $T = 1700$ K.

practical applications of the continuum approach. In many problems the transport coefficients are assumed to be experimentally determined constants, depending only on the temperature and density of fluid, but in more complex situations, transport coefficients can depend only on local behavior, an example being the dependence of shear viscosity on the velocity gradient [93]. Some of the most familiar transport properties are diffusion coefficients and shear viscosity, and dynamic structure factor for more advanced studies.

Diffusion is the name of the phenomenon in which molecules move from one part of a system to another through a process depending on the force occurring from the imbalance between different parts of the system [69]. Diffusion coefficient, D, is defined by Fick's law relating mass flow to density gradient in a
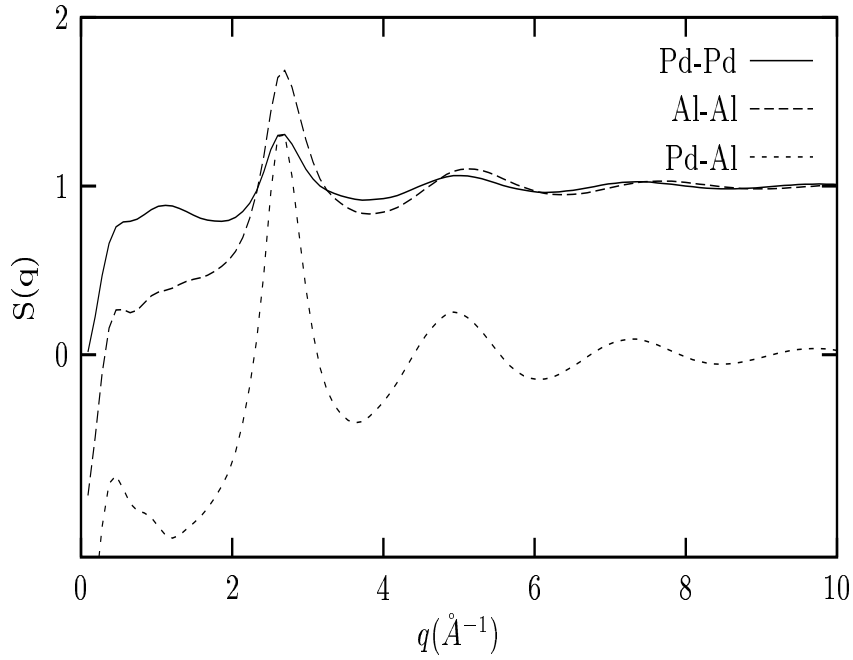
53

Figure 5.14: Simulated static structure factor of $Pd_{0.2}Al_{0.8}$ alloy at $T = 1100\ K$.

Table 5.4: Diffusion coefficients at different temperatures. Values, which are given in the columns headed by "Refs." , are taken from experimental or first principle calculations of corresponding authors.

T	D_{Pd}		D_{Al}		D_{Pd-Al}			
(K)	$(cm^2 s^{-1}) \times 10^{-5}$		$(cm^2 s^{-1}) \times 10^{-5}$		$(cm^2 s^{-1}) \times 10^{-5}$			
	Q-SC	Refs.	Q-SC	Refs.	$Pd_{0.8}Al_{0.2}$	$Pd_{0.6}Al_{0.4}$	$Pd_{0.4}Al_{0.6}$	$Pd_{0.2}Al_{0.8}$
943			15.579	7.476[72]				
985			16.077	4.16[77]				
1000								6.217 $(1-1)$
								9.441 $(2-2)$
1023			17.878	9.230[72]				7.793 $(1-1)$
								11.462 $(2-2)$
1200			0.37				5.285	8.641 $(1-1)$
							7.537	13.102 $(2-2)$
1400			28.518			5.134	7.719	11.991 $(1-1)$
						6.609	10.423	17.882 $(2-2)$
1600			35.155		4.654	6.706	10.181	14.823 $(1-1)$
					5.290	9.138	14.081	22.052 $(2-2)$
1800			43.422		6.501	8.615	12.973	18.364 $(1-1)$
					7.371	11.701	18.302	27.572 $(2-2)$
1853	5.029	4.037[44]						
2000	6.192		51.430		8.155	11.162	15.117	21.956 $(1-1)$
					9.461	15.213	21.642	33.252 $(2-2)$
2200	7.683		60.32		10.183	11.402	18.296	26.051 $(1-1)$
					11.846	17.524	25.932	38.642 $(2-2)$
2500	10.424		70.310		13.213	17.013	23.081	31.892 $(1-1)$
					15.494	21.333	33.155	48.304 $(1-1)$
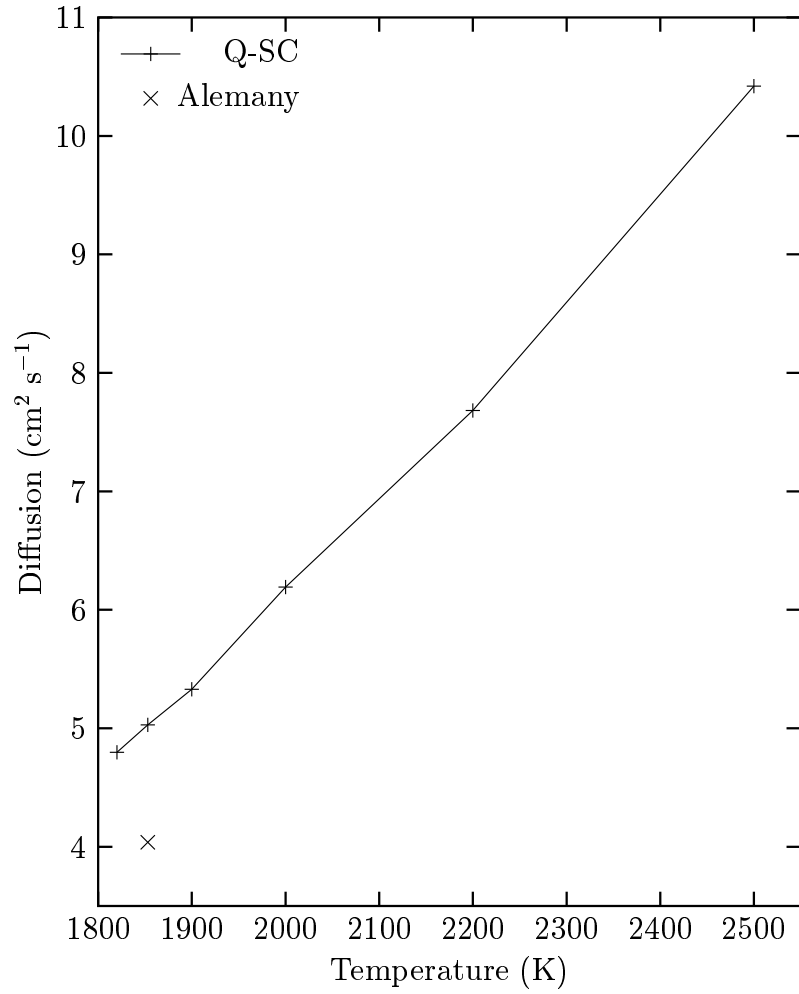
Figure 5.15: Diffusion coefficients from Alemany's [44] work at ($\rho(T = 1853K) = 10496.78 \ kg.m^{-3}$) and our simulated results by Q-SC potential ($\rho(T = 1000K) = 9664.06 \ kg.m^{-3}$).

Figure 5.16: Experimental and simulated diffusion coefficients of liquid Al a-EMD data ($\rho(T = 1000K) = 2268\ kgm^{-3}$) [72], b- Stokes-Einstein [105], c-Sutherland-Einstein [105], d-Universal Scaling Law [106], e- Alfe *et al.*($\rho = 2350\ kg.m^{-3}$) [107], f- Alfe *et al.*($\rho = 2470\ kg.m^{-3}$) [107], Q-SC ($\rho(T = 1000K) = 2208.81\ kg.m^{-3}$).

continuous system [71]. For large t we have the Einstein expression [71].

$$D = \lim_{t \to \infty} \frac{1}{6Nt} \left\langle \sum_{j=1}^{N} [\mathbf{r}_j(t) - \mathbf{r}_j(0)]^2 \right\rangle. \qquad (5.3)$$

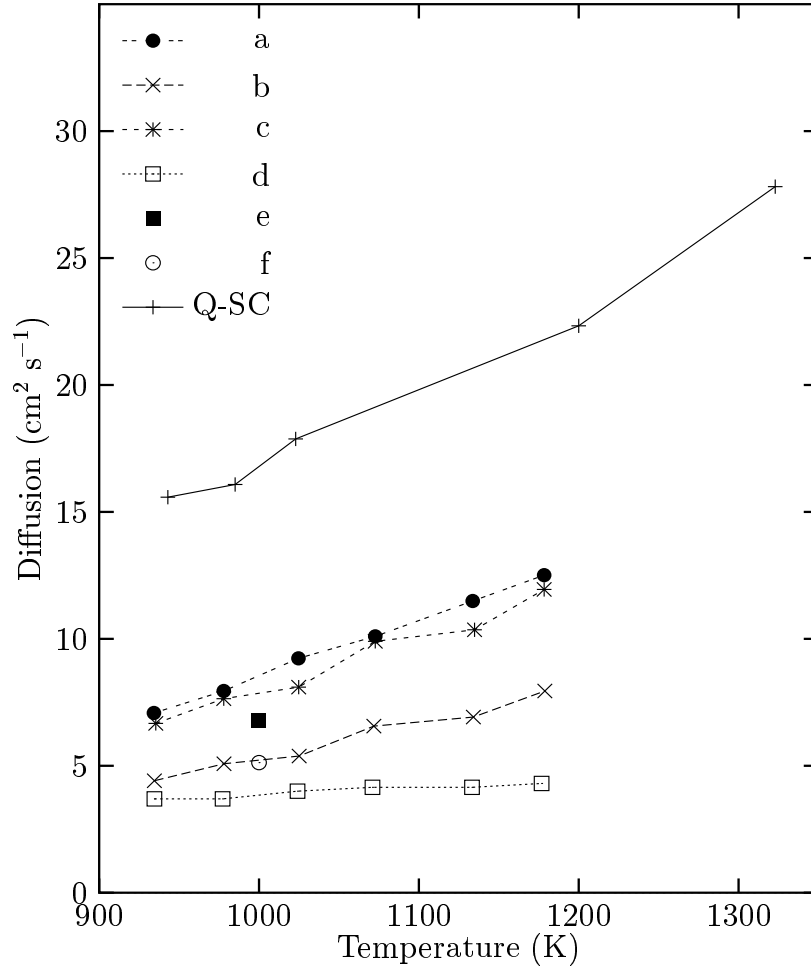The diffusion coefficients obtained from Einstein expression (5.3) are given in Table 5.4 for Pd and Al liquid metals, and Fig. 5.15 and Fig. 5.16 display the diffusion coefficients calculated by MD method with Q-SC potential.

The experimental data is hard to find for diffusivity of Pd. But our results agree with the MD data calculated by Green-Kubo and Einstein relations with 20% error percentage [44] as seen in Fig. 5.15. There is a range of diffusion coefficients found experimentally, theoretically, and by simulation in Fig. 5.16. Depending on the aluminum parametrization, diffusion coefficients are low compared with the published experimental results [72, 76], but they have reliable values. The comparison shows the success of Q-SC potential parameters.

Diffusion coefficients have been calculated for Pd and Al and $Pd_{0.8}Al_{0.2}$, $Pd_{0.6}Al_{0.4}$, $Pd_{0.4}Al_{0.6}$, and $Pd_{0.2}Al_{0.8}$ alloys in different temperatures. The results are exhibited in Table 5.4. Additionally, available results obtained by experiment or theory, or first-principles simulation are given in the Table 5.4. We are able to find experimental and theoretical data published on self diffusion of Al, and self diffusion of Pd, but to the best of our knowledge, there is no experimental or calculated data on diffusion of Pd-Al alloys. Because of lack of the experimental or calculated data, we list our simulated self diffusion data on Pd-Al alloy without any comparison in Table 5.4.

In Table 5.4; the rows shown as $(1 - 1)$ include Pd-Pd species of Pd-Al alloy

and $(2-2)$ include the Al-Al species. The data given for pure Al, in the "Refs." column have been taken from Cherne [72] and they are theoretical calculation results. Similarly, the data given for pure Pd in the "Refs." column have been taken from Alemany [44] and they are also theoretical results.

5.6 Shear Viscosity
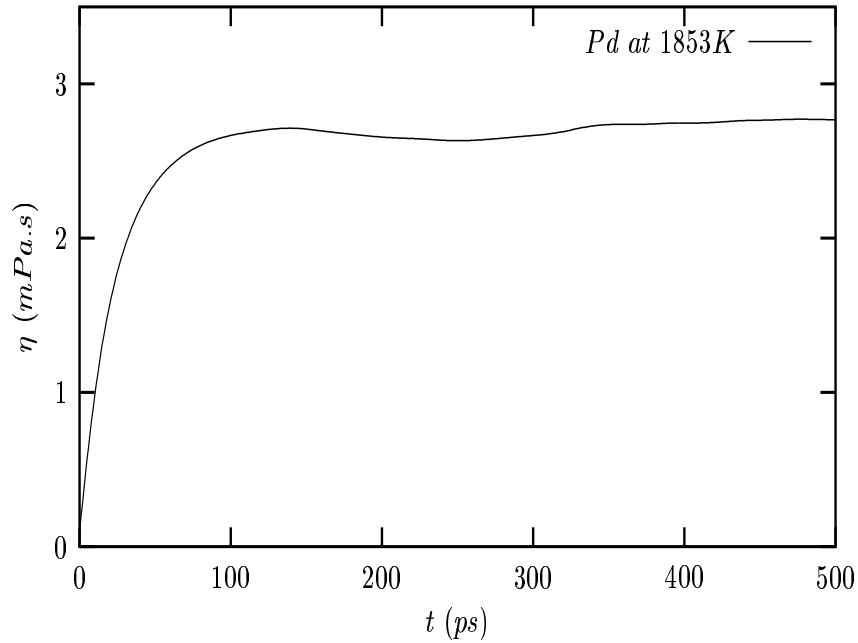
Figure 5.17: Viscosity integral of stress auto correlation function for liquid Pd ($T = 1853\ K$). Reference data is taken from Alemany [44].

Viscosity is defined as a measurement of resistance to flow [69]. Two adjacent layers slip past each other, each exerts a frictional resistive force on the other, and this internal friction gives rise to viscosity. The shear viscosity η is defined by the Navier-Stokes theorem [71], which defines shear viscosity and bulk viscosity together.

There are two expressions mostly used in the calculation of shear viscosity
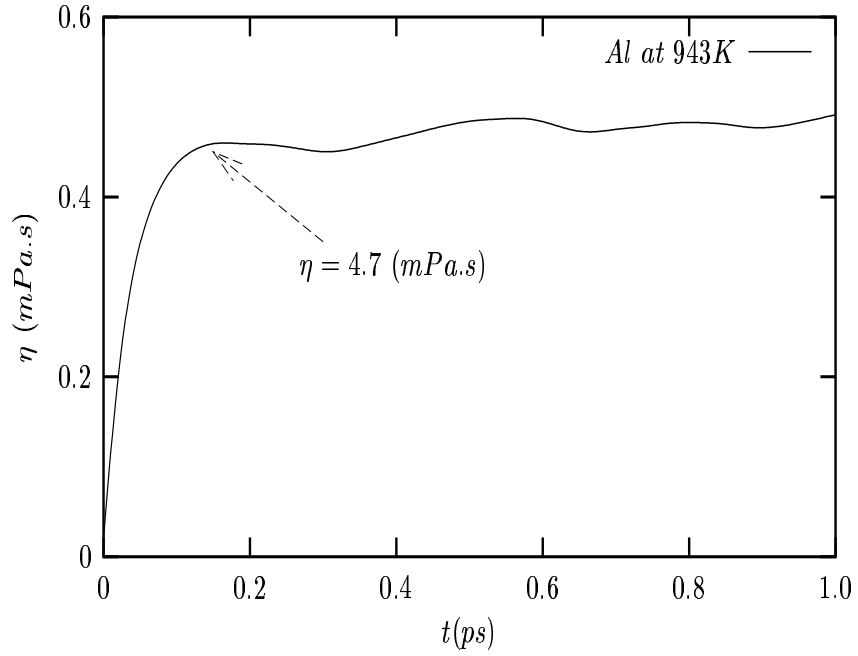
Figure 5.18: Viscosity integral of stress auto correlation function for liquid Al $(T = 943\ K)$.

of fluids. The expression which is analogous to the Einstein relation (EC. 5.3) [71, 108] is;

$$\eta = \lim_{t \to \infty} \frac{1}{6k_B T V t} \left\langle \sum_{x<y} \left[\sum_j m_j r_{xj}(t) v_{yj}(t) - \sum_j m_j r_{xj}(0) v_{yj}(0) \right]^2 \right\rangle, \qquad (5.4)$$

where $\sum_{x<y}$ denotes a sum over the three pairs of distinct vector components (xy, yz, and zx) and it is used to improve the statistics. This expression can not be used with periodic boundary conditions because they violate the invariance assumed in the derivation [109]. An alternative relation is given by the Green-Kubo expression which is based on the integrated auto-correlation function of the pressure tensor[71],

$$\eta = \frac{V}{3k_b T} \int_0^\infty \left\langle \sum_{\alpha<\beta} P_{\alpha\beta}(t) P_{\alpha\beta}(0) \right\rangle dt, \qquad (5.5)$$

where $\alpha\beta = xy, yx, xz$, and $\left\langle \sum_{\alpha<\beta} P_{\alpha\beta}(t) P_{\alpha\beta}(0) \right\rangle$ is the stress auto-correlation

59

function,

$$P_{\alpha\beta} = \frac{1}{V} \left[\sum_j m_j v_{xj} v_{yj} - \sum_{i \neq j} r_{xij} f_{yij} \right].$$ (5.6)
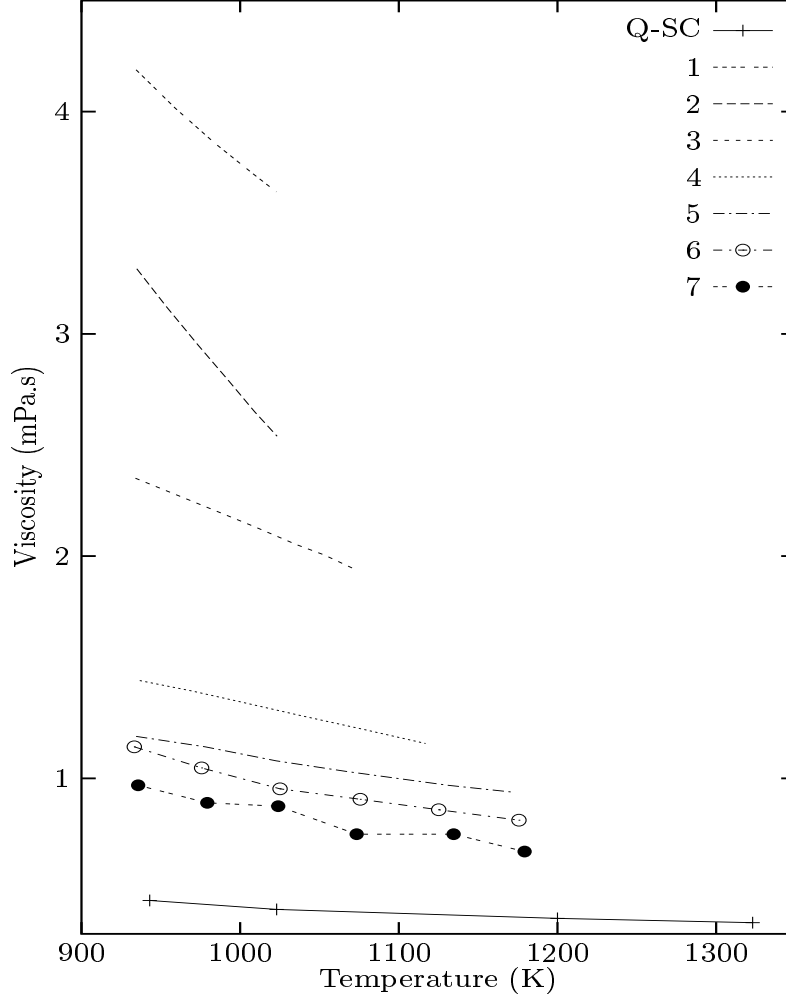
Figure 5.19: Shear viscosities for liquid Al as a function of temperature. (1,2,3,4 and 5 corresponds experimental data from Ref. [76] where 1,2,3,4 and 5 correspond to Refs. [110]-[114], 6- is calculated from NEMD, and 7- is calculated from equilibrium MD simulations) [72, 76].

Eqs. (5.4) and (5.5) are completely identical. Components of pressure tensor, $P_{\alpha\beta}$, have already been calculated during our simulations, so we used Eq. (5.5) to calculate the shear viscosities of both metals. Fig. 5.17 and Fig. 5.18 display

the viscosity integrand for Pd ($T = 943\ K$) and Al ($T = 1853\ K$), respectively.

Table 5.5: Shear viscosities at different temperatures. Experimental values, included column titled by "Refs." are taken from experimental or first principle calculations [44, 72].

T	$\eta_{Pd}(mPa.s)$		$\eta_{Al}(mPa.s)$		$\eta_{PdAl}(mPa.s)$			
(K)	Q-SC	Refs.	Q-SC	Refs.	$Pd_{0.8}Al_{0.2}$	$Pd_{0.6}Al_{0.4}$	$Pd_{0.4}Al_{0.6}$	$Pd_{0.2}Al_{0.8}$
943			0.47	1.20[72]				
1000			0.42	0.87[72]				
1200			0.37	0.67[72]				
1400			0.33					
1600			0.31		2.52	1.60	1.02	0.50
1800			0.28		1.93	1.33	0.89	0.49
1853	2.69	2.30[44]						
1900	2.57				1.63			
2000	2.50		0.27		1.55	1.21	0.78	0.47
2200	1.93		0.26		1.25	1.08	0.74	0.46
2500	1.68		0.24			0.92	0.60	0.43

We have calculated the shear viscosities of Pd and Al and Pd-Al alloys in different concentrations. There are a few calculations published for Pd [44] but many for Al. The experimental and simulated results are shown on Fig. 5.19, so we do not insert this data into the Table 5.5. To the best of our knowledge, there is no experimental or theoretical datum on the shear viscosities of Pd-Al.

The data given for pure Al in the "Refs." columns of Table 5.5 have been taken from Cherne [72] and it is a theoretical result. Similarly, the data given for pure Pd in the "Refs." columns have been taken from Alemany [44] and it is also a theoretical result. There is a range of experimental viscosities for Al in the paper by Cherne [72] and the results show that MD simulation is successful for viscosity of Pd and Al.
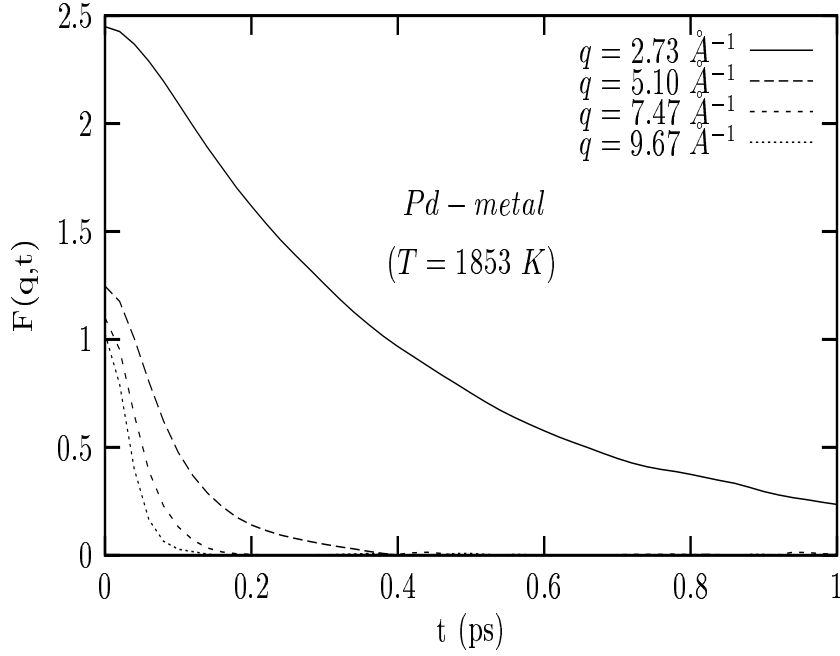
Figure 5.20: Intermediate scattering function of liquid Pd ($\rho = 9680.7 \ kg.m^{-3}$).

5.7 Intermediate Scattering Function

Intermediate scattering function $F(\mathbf{q}, t)$, which is a density-density correlation function, is the time dependent picture of a material in $\mathbf{q}$ space. MD simulation of $F(\mathbf{q}, t)$ by using $Q - SC$ potential gives good results in agreement with published data for Al[77].

We analyzed the molecular dynamics results for the intermediate scattering function, which is given by [57, 92, 115],

$$\begin{aligned} F(\mathbf{q}, t) &= \int d\mathbf{r} \exp\left(-i\mathbf{q}\mathbf{r}\right) \\ &= \frac{1}{N} < \rho_{-\mathbf{q}}(t).\rho_{\mathbf{q}} >, \end{aligned} \tag{5.7}$$

where $\rho_{\mathbf{q}}(t)$ is the time-dependent Fourier component of the density of the system,

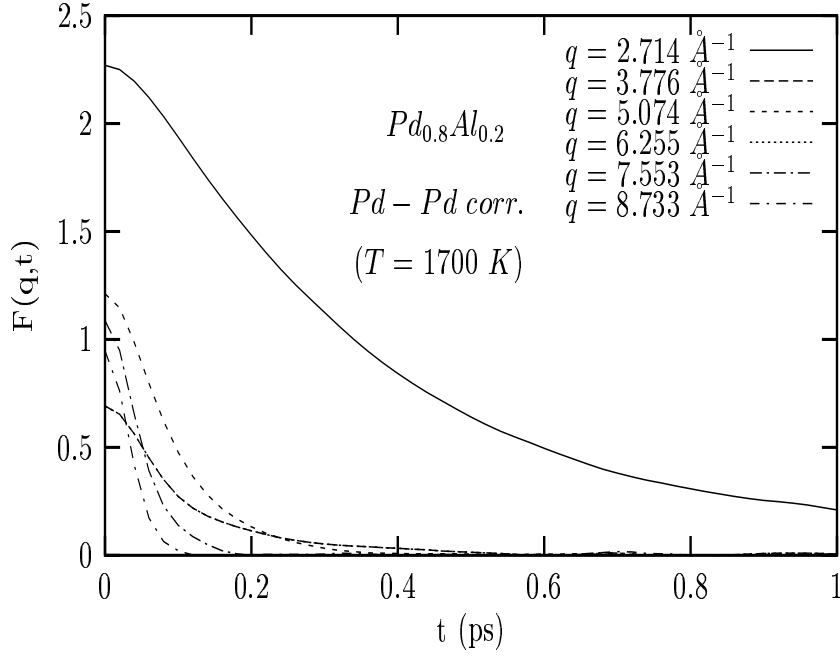Figure 5.21: Partial intermediate scattering function for Pd-Pd species of liquid $Pd_{0.8}Al_{0.2}$ alloy ($\rho = 8114.5 \ kg.m^{-3}$).

given by the following relation:

$$\rho(\mathbf{r}, t) = \sum_{j=1}^{N} \exp(-i\mathbf{q}.\mathbf{r}_j(t)). \tag{5.8}$$

Periodic boundary conditions with minimum image method satisfy the time dependent continuity of $F(\mathbf{q}, t)$. Because of the periodic boundary conditions only certain wave vectors are allowed

$$\mathbf{q} = \frac{2\pi}{L}(\mathbf{n}_1, \mathbf{n}_2, \mathbf{n}_3), \tag{5.9}$$

where n_i are integers and each wave vector with $n_1 \geq n_2 \geq n_3$, contributes to all possible symmetries of $\mathbf{q}$ values. Since our system is an isotropic system, $F(\mathbf{q}, t)$ depends only on the magnitude of $\mathbf{k}$ and not on its direction. Thus, $F(\mathbf{q}, t)$ is a function only of the wavenumber $q = |\mathbf{q}|$ and t.

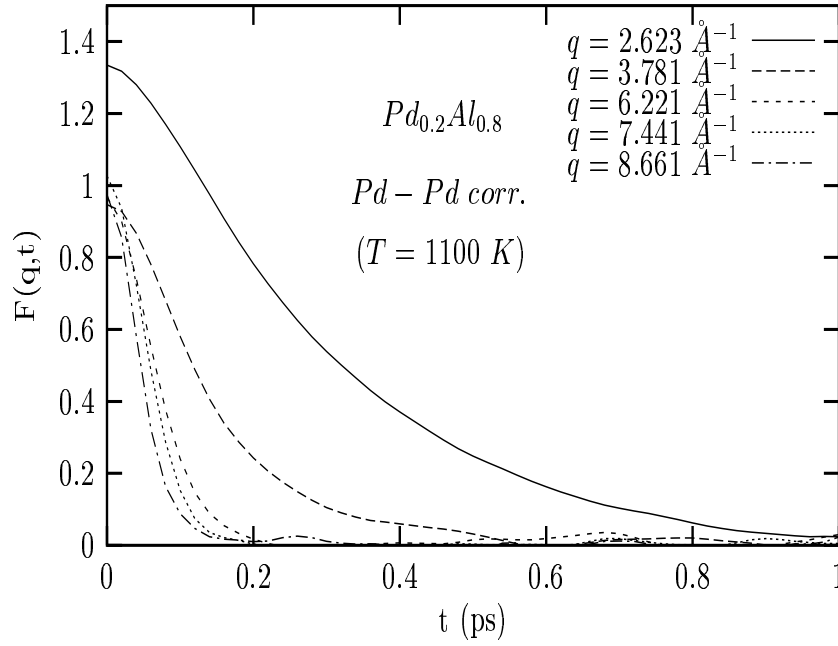$F(q, t)$ has been averaged over 500 time origins. Although trajectory file has

63

Figure 5.22: Partial intermediate scattering function for Pd-Pd species of liquid $Pd_{0.2}Al_{0.8}$ alloy ($\rho = 3675.8\ kg.m^{-3}$).

5000 time origins, each 10 of the original time points has been used as a time origin. $\Delta t = 0.002\ ps$ have been selected as the time increment. As a result, calculations have been made on 1 ps time scale. The q values have been selected from the extremum points of $S(q)$ curve of the selected metal or alloy at the given temperatures. These points are given in Table 5.6 for the relevant temperatures.

In Table 5.6, q values of the extremum points are given by corresponding $S(q)$ values of Pd and Al. Extremum points of alloys are selected from total structure factors of $Pd_{0.8}Al_{0.2}$ and $Pd_{0.2}Al_{0.8}$ alloys, but we have calculated four different structure factors for each alloy depending on the number of components of alloy. These are the structure factors for Pd-Pd and Al-Al self species, structure factors for Pd-Al distinct species, and structure factors for Pd-Al in which both species interacting randomly (total structure factors).
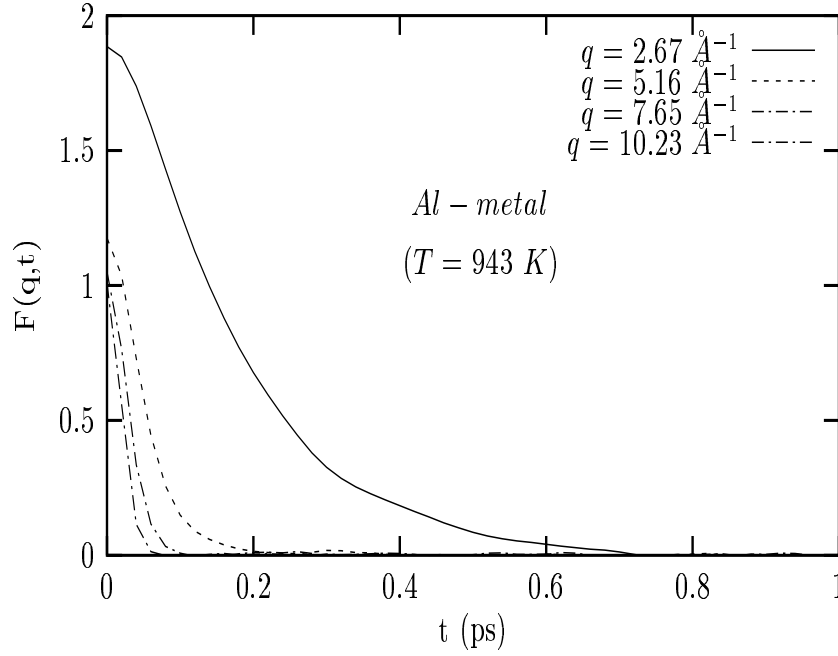
Figure 5.23: Intermediate scattering function of liquid Al ($\rho = 2232.7 \ kg.m^{-3}$).

Fig. 5.20 and Fig. 5.23 represent the time dependent behavior of intermediate scattering functions of Pd and Al pure metals. Figures 5.21, 5.22 represent the time dependent behavior of intermediate scattering functions of Pd-Pd correlation for $Pd_{0.8}Al_{0.2}$ and $Pd_{0.2}Al_{0.8}$ alloys and Figs. 5.24, 5.25 represent the time dependent behavior of intermediate scattering functions of Al-Al interaction for $Pd_{0.8}Al_{0.2}$ and $Pd_{0.2}Al_{0.8}$ alloys, respectively. As it is seen from Fig 5.20 and Fig. 5.23, intermediate scattering functions of Pd and Al have a smooth time dependent shape approaching to zero as in all transport correlations. We compared the behavior of Pd-Pd and Al-Al self components of $Pd_{0.8}Al_{0.2}$ and $Pd_{0.2}Al_{0.8}$ alloys with Pd and Al to see the behavior of atoms in alloy.

In Fig. 5.22 the starting point of $F(q, t)$ has smaller values due to decreasing Pd concentration. This is an expected result, because of the decreasing probability of finding a Pd atom around origin at time zero. In the pure metal and $Pd_{0.8}Al_{0.2}$

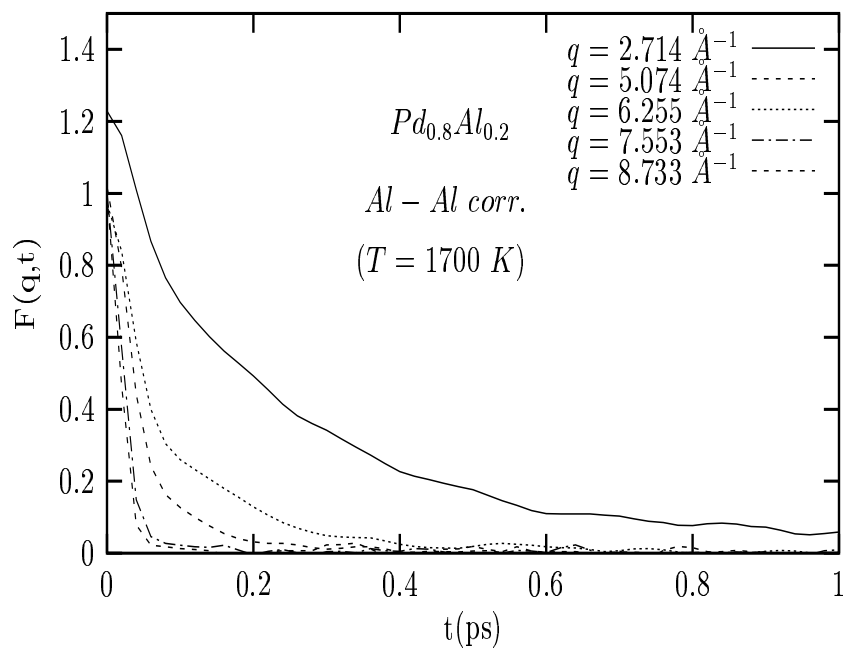Figure 5.24: Partial intermediate scattering function for Al-Al species of liquid $Pd_{0.2}Al_{0.8}$ alloy ($\rho = 3675.8$ $kg.m^{-3}$).
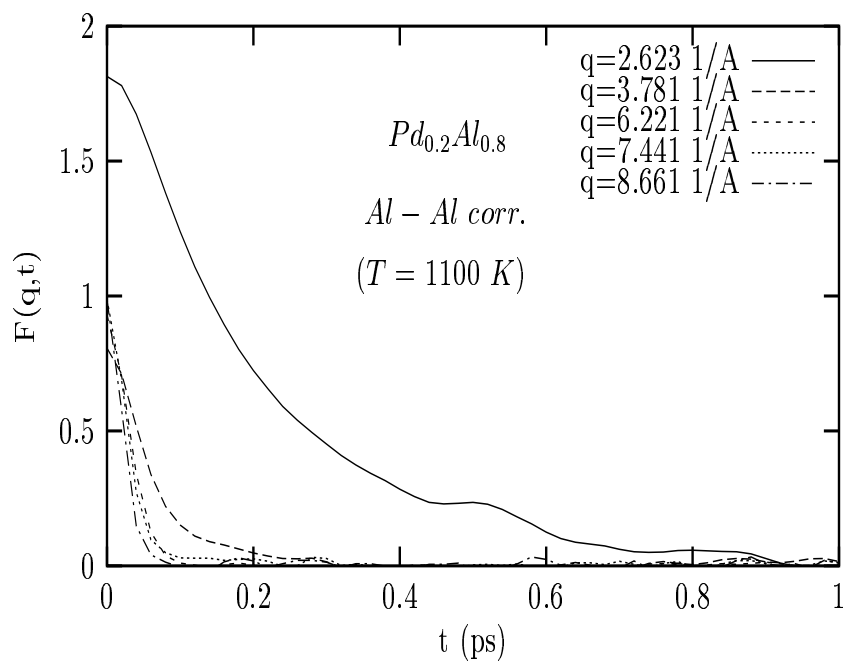

Figure 5.25: Partial intermediate scattering function for Al-Al species of liquid $Pd_{0.8}Al_{0.2}$ alloy ($\rho = 8114.5$ $kg.m^{-3}$).

Table 5.6: Selected q values of Pd and Al and $Pd_{0.8}Al_{0.2}$ and $Pd_{0.2}Al_{0.8}$ alloys at the extremum points of $S(q)$. q values of Pd and Al are given by the $S(q)$ and extremum points of alloys are selected from their total structure factor.

Pd (1853 K)		Al (943 K)		$Pd_{0.8}Al_{0.2}$ (1700 K)		$Pd_{0.2}Al_{0.8}$ (1100 K)	
q ($\mathring{A}^{-1}$)	$S(q)$	q ($\mathring{A}^{-1}$)	$S(q)$	q ($\mathring{A}^{-1}$)	$S(q)$	q ($\mathring{A}^{-1}$)	$S(q)$
2.73	2.448	2.67	1.885	2.714	2.30	2.662	2.11
3.79	0.631	3.82	0.745	3.776	0.64	3.781	0.71
5.10	1.246	5.16	1.175	5.074	1.24	5.001	1.18
6.28	0.875	6.31	0.917	6.255	0.87	6.221	0.90
8.78	0.938	7.65	1.051	7.553	1.08	7.441	1.05
9.67	1.027	8.89	0.987	8.733	0.94	8.661	0.96

and $Pd_{0.2}Al_{0.8}$ alloy cases both Pd and Al species have strong correlations at time $t = 0$, but this $F(q, t)$ correlations decrease to zero in time. The small oscillations in the tails of curves are noises. These noises can be reduced by increasing the number of atoms in the simulation.

When we compare the intermediate scattering function behavior of Pd and Al, we can say that Pd atoms have stronger correlations. These correlations are also much more long lasting than Al atoms' correlations.

5.8 Bulk modulus

Bulk modulus values, in different concentrations and temperatures, have been calculated both from elastic constants and $F(q, t)$ functions. Bulk modulus has a special importance for discussing the efficiency of simulation. Although Ebbsjö et al. [77] claimed that the bulk modulus calculated from S(0) value is not reliable, we see that bulk modulus calculated from $F(q, t)$ functions in the smallest
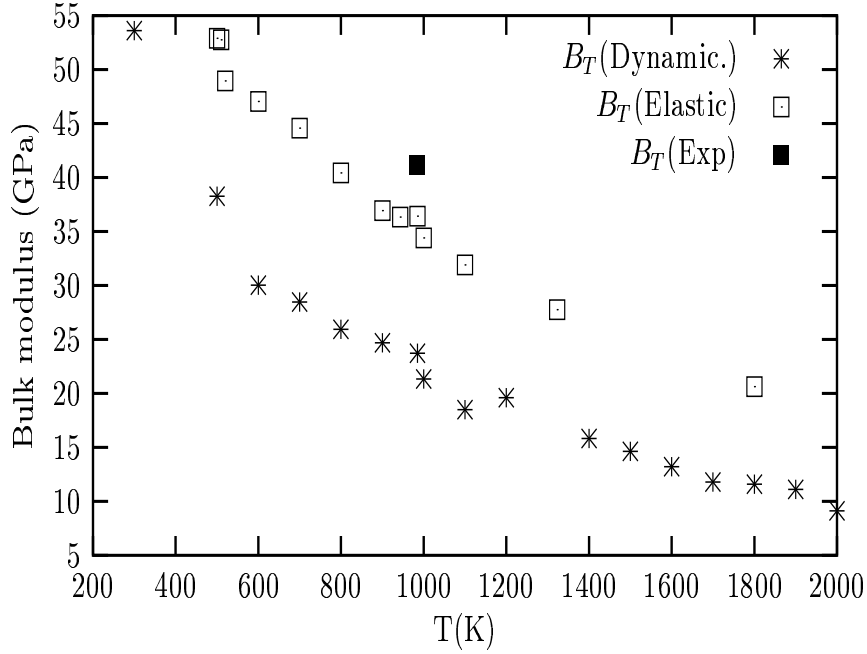
Figure 5.26: Experimental and simulated bulk modulus of Al.

hyrodynamics limit ($q = 0.266 \ \AA^{-1}$) is reliable. The reason for Ebbsjö's [77] claim

is that the exact estimation of S(q) in the $t \to 0$ limit is not possible from MD

simulations, because S(q) has some elusive behavior in the smallest hyrodynam-

ics limit, but $F(q, t)$ does not have this disadvantage. Fig. 5.26, Fig. 5.27 and

Fig. 5.28 illustrate the bulk modulus of Pd, Al, and $Pd_{0.6}Al_{0.4}$ alloys, respectively.

Initial value of intermediate scattering function, $F(q, 0)$, is used to calculate

compressibility of Pd and Al elements and Pd-Al alloy at the hydrodynamic limit

($q \ll 1, \quad t \to 0$) by using following expression,

$$\kappa_T = \frac{F(q, 0)}{\rho k_B T}. \tag{5.10}$$

In Fig. 5.26, bulk modulus values calculated from elastic constants seem closer

to the experimental data [116] compared to that of the values calculated from

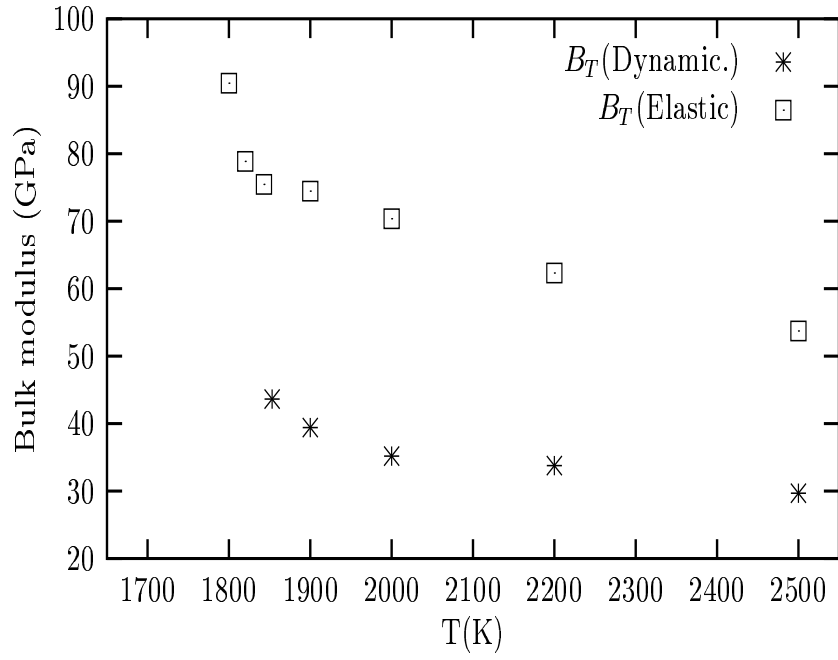$F(q, 0)$ functions. As it is discussed in the third chapter, bulk modulus is one

Figure 5.27: Bulk modulus of Pd calculated from elastic constants and $F(q, t)$ function.
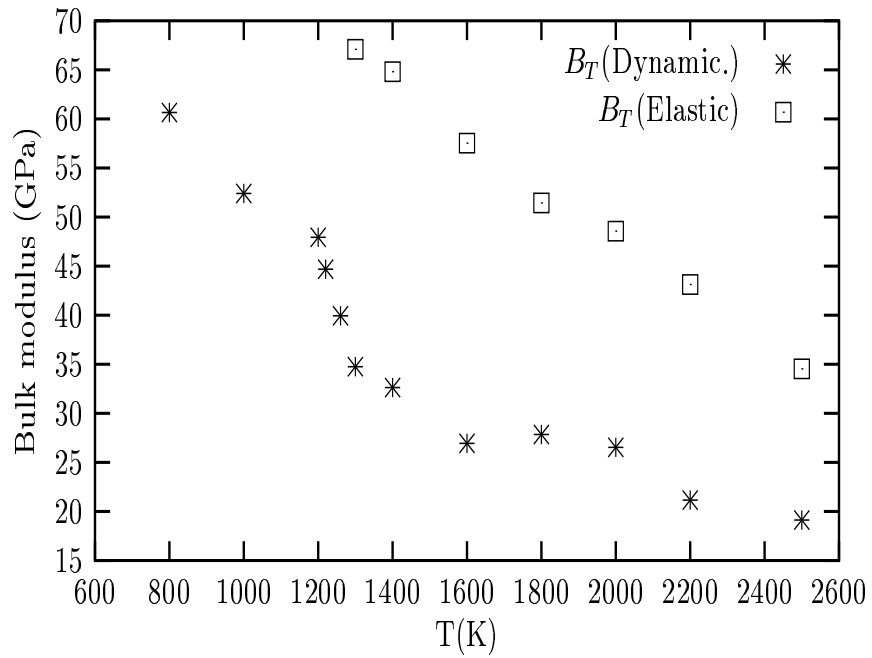

Figure 5.28: Bulk modulus of $Pd_{0.6}Al_{0.4}$ alloy calculated from elastic constants and $F(q, t)$ function.
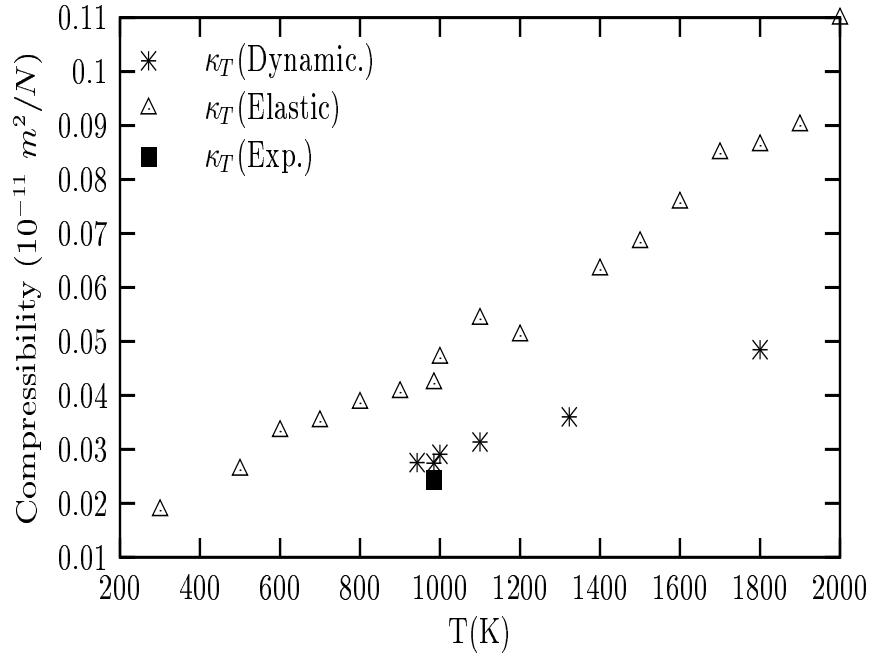
Figure 5.29: Experimental and simulated compressibility of Al.

of the properties which is used in the optimization of potential. This explains

why the bulk modulus is found closer to experimental value rather than the value

found by using F(q,0) functions.

5.9 Compressibility

Compressibility is the inverse of bulk modulus. Compressibility is calculated

from elastic constants and $F(q,t)$ functions in the hydrodynamic limit. There

are some differences between them and these differences explain the behavior of

potential. Fig. 5.29, Fig. 5.30 and Fig. 5.31 illustrate the compressibility of Pd,

Al, and $Pd_{0.6}Al_{0.4}$ alloys, respectively.

As seen from Fig. 5.30 the compressibility calculated from elastic constants

is closer to experimental data [116] compared to that of the data obtained from

$F(q,t)$ function. The reason for this can be explained by the fitting method used,
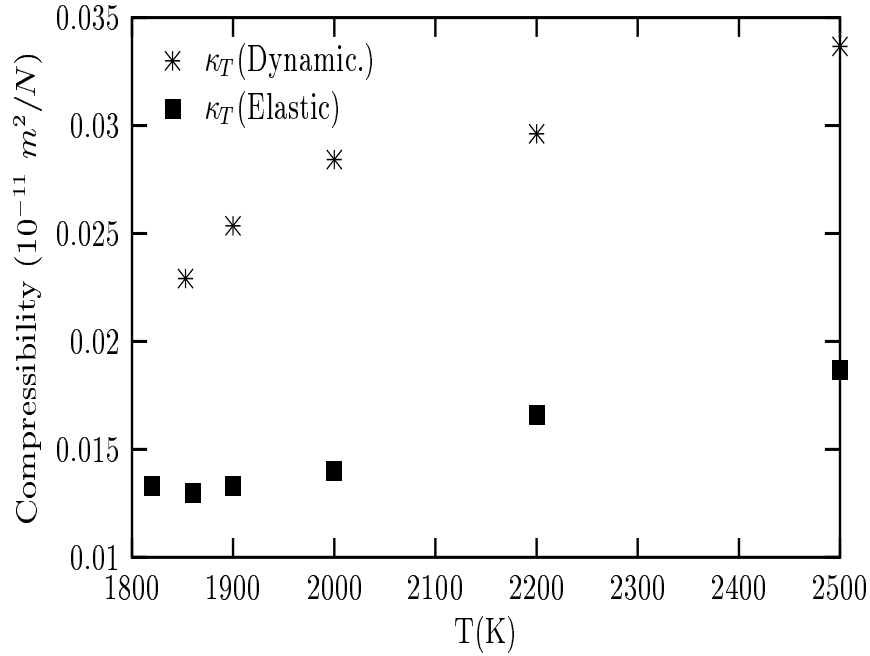
Figure 5.30: Compressibility of Pd calculated from elastic constants and $F(q,t)$ function.

as has already been mentioned in the previous section.

5.10 Dynamic structure factor

Determining the dynamic structure factor of a liquid metal is one of the most expensive and time consuming tasks since the working temperature is very high and thus measurement equipment needs very high technology. On the other hand the dynamic structure factor has a significant importance because of its relation to a very well known experiment, "inelastic scattering", and supplies very important information. The inelastic scattering is explained in detail by Hansen [57].

Dynamic structure factor, $S(\mathbf{q}, \omega)$ is a spatial Fourier transform of $F(\mathbf{q}, t)$ and it is given by the following equation.

$$S(\mathbf{q}, \omega) = \frac{1}{2\pi} \int_{-\infty}^{\infty} F(\mathbf{q}, t) \exp(i\omega t) dt, \qquad (5.11)$$

71

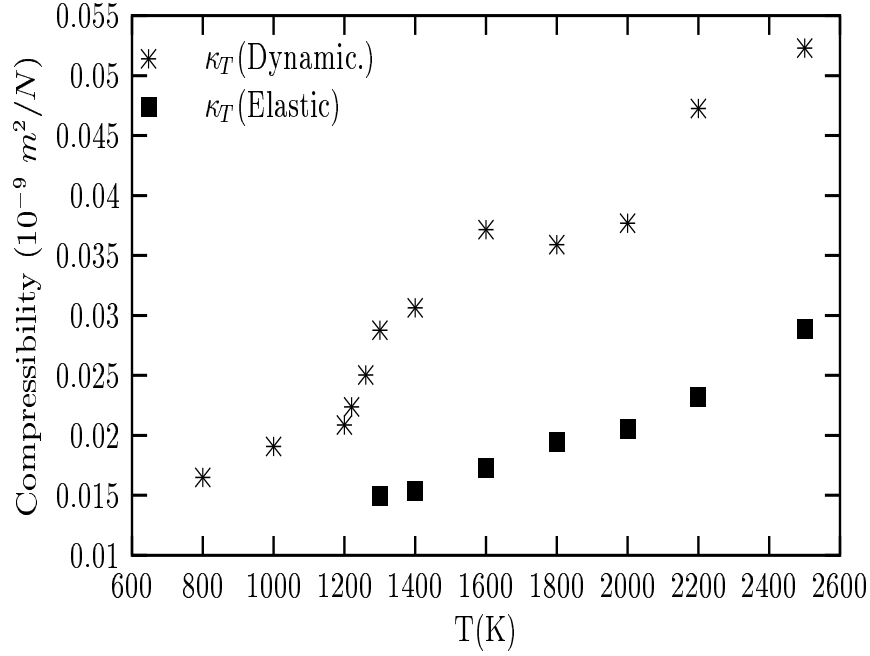Figure 5.31: Compressibility of $Pd_{0.6}Al_{0.4}$ alloy calculated from elastic constants and $F(q,t)$ function.

where $F(\mathbf{q}, t)$ is the intermediate scattering function and is given by Eq. (5.7).

In alloy systems, dynamic structure factor can be defined to describe self and distinct species. It is given for two component liquid alloys by the following expression [57, 90].

$$S_{\alpha\beta}(\mathbf{q}, \omega) = \frac{1}{2\pi} \int_{-\infty}^{\infty} F_{\alpha\beta}(\mathbf{q}, t) \exp(i\omega t) dt, \qquad (5.12)$$

where α and β represent components of the alloy. $F_{\alpha\beta}(\mathbf{q}, t)$ is given as

$$F_{\alpha\beta}(\mathbf{q}, t) = \frac{1}{N} < \rho_{-\mathbf{q}^{\alpha}}(t).\rho_{\mathbf{q}^{\beta}} > . \qquad (5.13)$$

$S(\mathbf{q}, \omega)$ has been calculated directly from trajectory data, which are products of EVN ensemble MD calculations.

Because of isotropy of our system, $S(\mathbf{q}, \omega)$ depends only on the magnitude of $\mathbf{k}$ and not on its direction. Thus, $S(\mathbf{q}, \omega)$ is a function of the wavenumber
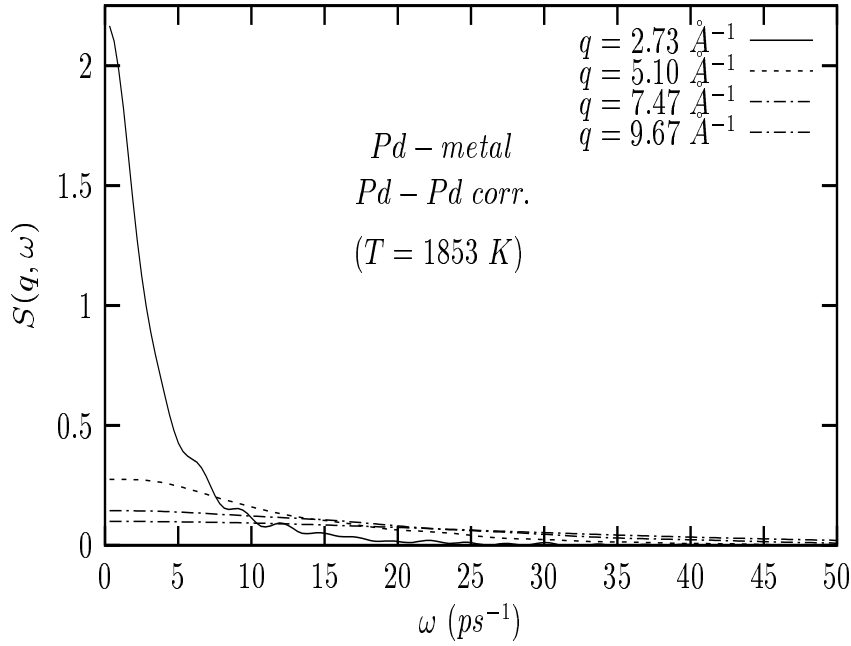
Figure 5.32: Dynamic structure factor for Pd-Pd species of liquid Pd ($\rho = 8114.5 \ kg.m^{-3}$).

$q = |\mathbf{q}|$ and ω. In the limit ($\mathbf{r}, \ t \rightarrow 0$), the particles in liquid move as if they were free, with a constant velocity $\mathbf{u}$. These conditions correspond to the limit ($q, \ \omega \rightarrow \infty$), where $S(q, \omega)$ behaves in the manner appropriate to an ideal gas. For a two component ideal gas the limiting form of $S(q, \omega)$ is easily derived. Since positions of different particles, represented by α and β, are uncorrelated in ideal gas ($S_{\alpha\beta}(q, \omega)$), the calculation of $S(q, \omega)$ is therefore equivalent to the calculation of self species $S_{\alpha\alpha}(q, \omega)$ and $S_{\beta\beta}(q, \omega)$.

Fig. 5.32 and Fig. 5.35 give the dynamical structure factor of liquid Pd and Al, respectively, in the large $\mathbf{q}$ region, namely in the free particle limit. Fig. 5.33 and Fig. 5.34 display the dynamical structure factor for Pd-Pd species of $Pd_{0.8}Al_{0.2}$ and $Pd_{0.2}Al_{0.8}$ alloys, respectively, and the dynamic structure factor for Al-Al species of $Pd_{0.8}Al_{0.2}$ and $Pd_{0.2}Al_{0.8}$ alloys are shown in the Fig. 5.36 and Fig. 5.37,
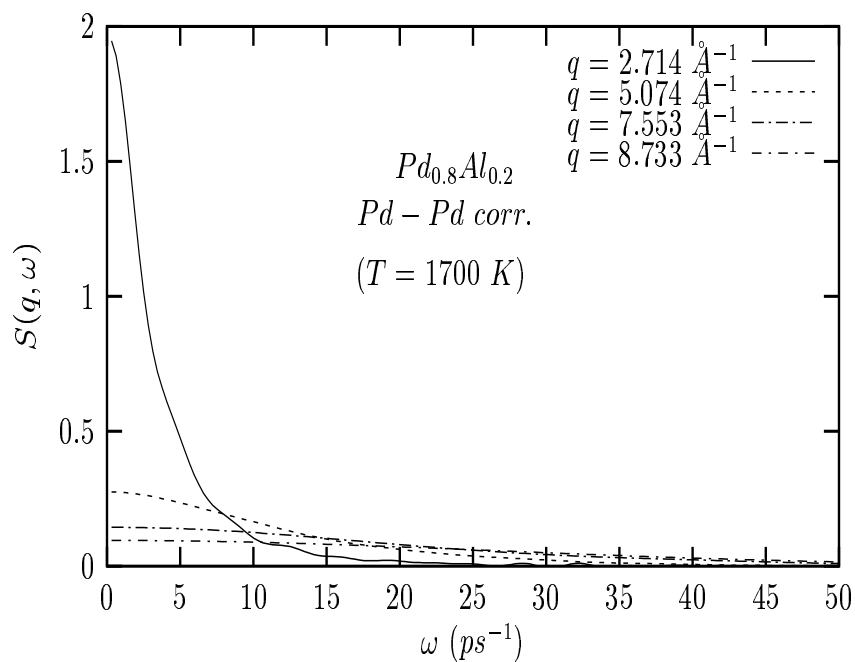
73

Figure 5.33: Partial dynamic structure factor for Pd-Pd species of liquid $Pd_{0.8}Al_{0.2}$ alloy ($\rho = 8114.5 \ kg.m^{-3}$).
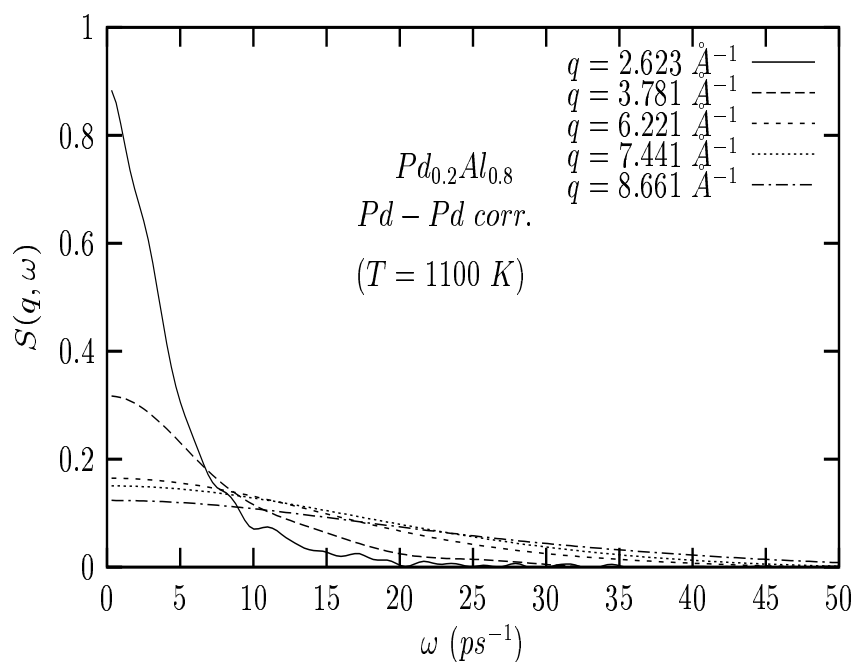
Figure 5.34: Partial dynamic structure factor for Pd-Pd species of liquid $Pd_{0.2}Al_{0.8}$ alloy ($\rho = 3675.8 \ kg.m^{-3}$).
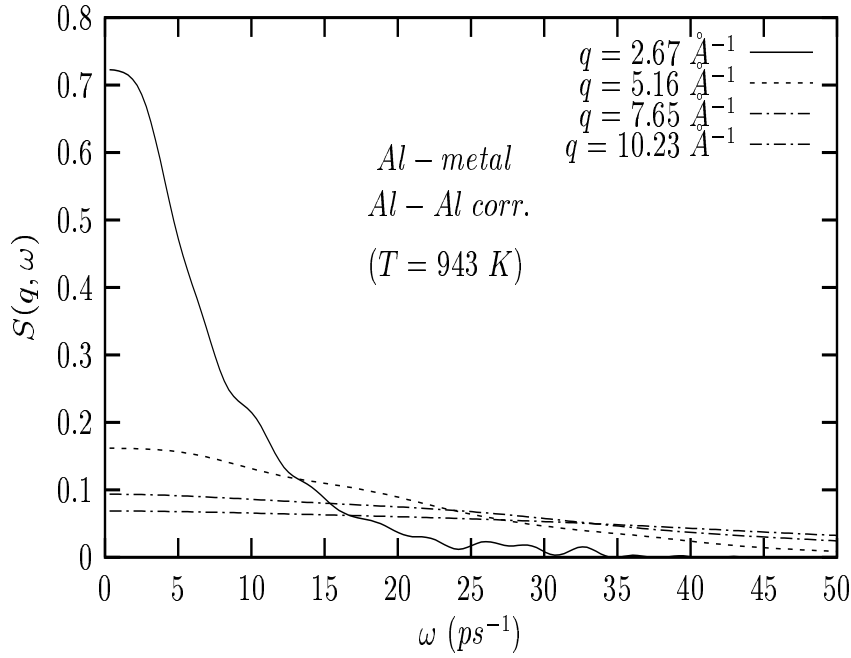
Figure 5.35: Dynamic structure factor for Al-Al species of liquid Al ($\rho = 2232.7 \ kg.m^{-3}$).

respectively.

Dynamic structure factor has an apparent tail with a clear starting point. In the free particle limit of, ($q, \ \omega \rightarrow \infty$), $S(q, \omega)$ has a smooth tail that approaches zero while ω increases. The decrease of $S(q, \omega)$ for Pd is faster than that for Al. The same is observed for Pd-Pd and Al-Al species in the $Pd_{0.8}Al_{0.2}$ and $Pd_{0.2}Al_{0.8}$ liquid alloys.

5.11 Hydrodynamic limit of $F(\mathbf{q}, t)$

Hydrodynamic limit of intermediate scattering function offers important information. Fig. 5.38 illustrates the comparison between $F(q, t)$ values, at $t \rightarrow 0$, and $S(q)$ (for $q = 0 - 1 \ \mathring{A}^{-1}$ range) in the hydrodynamic limit. It is expected that they would be nearly the same because $F(q, 0) = S(q)$ at the proper q value,
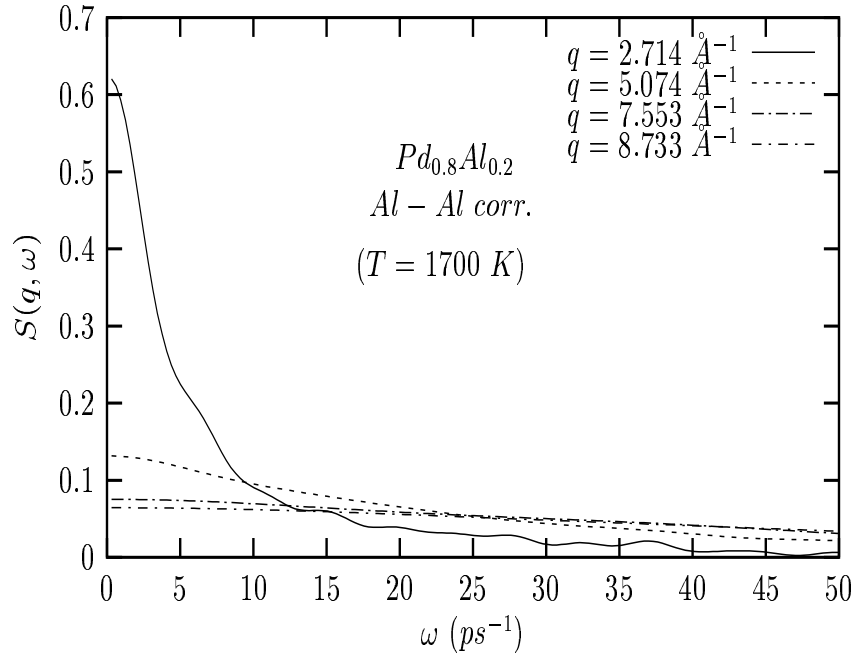
Figure 5.36: Partial dynamic structure factor for Al-Al species of liquid $Pd_{0.8}Al_{0.2}$ alloy ($\rho = 8114.5\ kg.m^{-3}$).

theoretically. But the differences, especially for alloy cases, are caused by the numerical errors. Fig. 5.39 displays $F(q,t)$ function which shows the time dependent structure of liquid Pd and Al and, Pd-Al alloys ($T = 1853\ K$). $F(q,t)$ has an oscillatory behavior in both Pd and Al.

5.12   Hydrodynamic limit of $S(q,\omega)$

It is seen that, analogous to previous studies [115, 78, 73], intermediate scattering function and dynamic structure factor for alloy system have a high value at the origin which shows that there are strong correlations between self species in the alloy system [78]. The magnitude of Al-Al dynamic structure factors are much greater than the magnitude of Pd-Pd dynamic structure factors as seen in the Fig. 5.40.
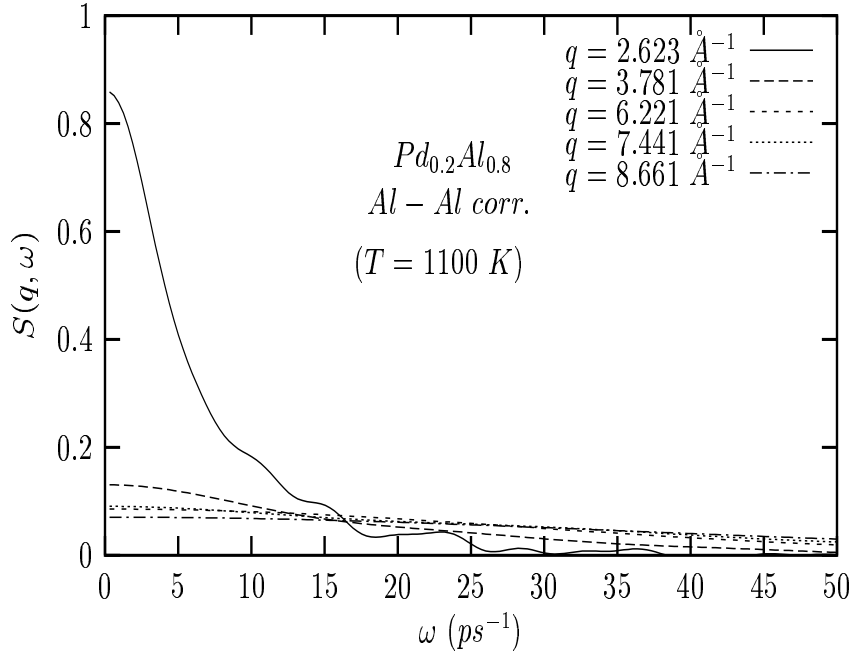
Figure 5.37: Partial dynamic structure factor for Al-Al species of liquid $Pd_{0.2}Al_{0.8}$ alloy ($\rho = 3675.8 \ kg.m^{-3}$).

Some noticeable peaks are observed in the hydrodynamic limit investigation of dynamic structure factor of Pd and Al. Although they are not as noticeable as in the metallic case, similar peaks are seen on the dynamic structure factor of $Pd_{0.8}Al_{0.2}$ and $Pd_{0.2}Al_{0.8}$ alloys for both Pd-Pd and Al-Al correlations. These peaks damp strongly at shorter wavelengths as in Fig. 5.40 and the high-frequency structures disappear, leaving only single-Lorentzian central peaks. The width of the central peaks first increase with q, but then show marked decreases at wave numbers close to the main peaks. This effect is called "de Gennes narrowing" [117] and corresponds to a dramatic slowing down in the decay of the density-density auto-correlation function $F(q, t)$ and has its origins in the strong spatial correlations.

These kinds of peaks were first observed by Bosse *et al.* [73] from MD simulation of the liquid $Li_{0.8}Pb_{0.2}$ alloy. Campa and Cohen [118] justified the existence of "fast sound" modes in binary mixtures of disparate-mass particles according to the kinetic theory. Neutron-scattering experiments of $Li_{0.8}Pb_{0.2}$ and $Li_{0.8}Tl_{0.2}$ alloys reflected the existence of these kinds of modes too. Anento and Padró [78, 119] studied the behavior of these peaks in detail. They noted that these $\omega^{ij}(q)$ peaks corresponds the propagating sound modes with velocity of sound in metal, c_s[78]. $\omega^{ij}(q)$ modes are seen in Fig. 5.41. The $\omega^{ij}(q)$ could only be observed for the $0.2 - 0.65$ $\mathring{A}^{-1}$ values of the q vector. $\omega^{ij}(q)$ values are evaluated for both Pd and Al.
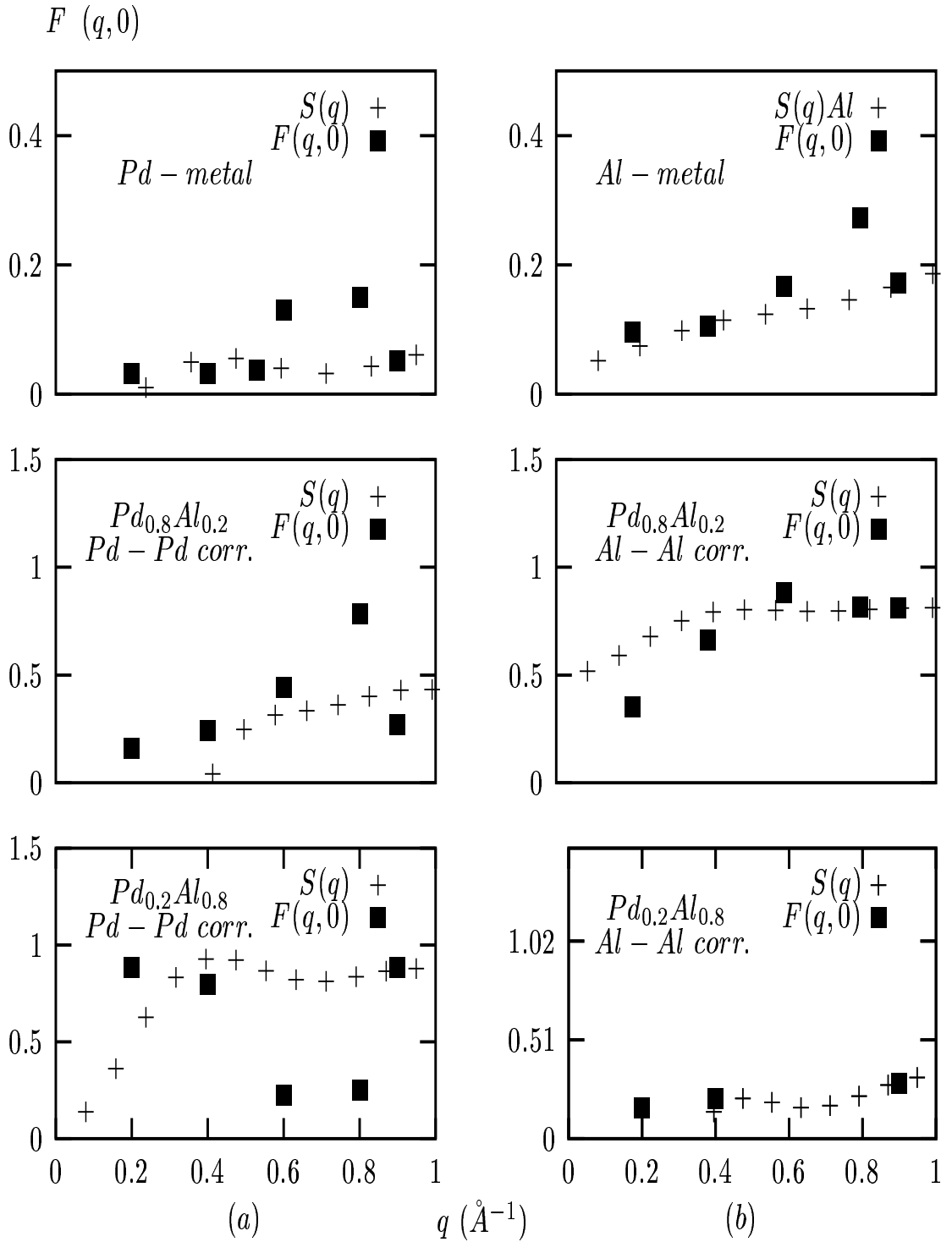
Figure 5.38: Comparison between $F(q, 0)$ and $S(q)$ values of (a) Pd-Pd self species correlation of liquid Pd metal, and $Pd_{0.8}Al_{0.2}$ and $Pd_{0.2}Al_{0.8}$ alloys from top to bottom respectively, and (b) Al-Al self species correlation of liquid Al metal, and $Pd_{0.8}Al_{0.2}$ and $Pd_{0.2}Al_{0.8}$ alloys from top to bottom, respectively ($T = 1853\ K$).
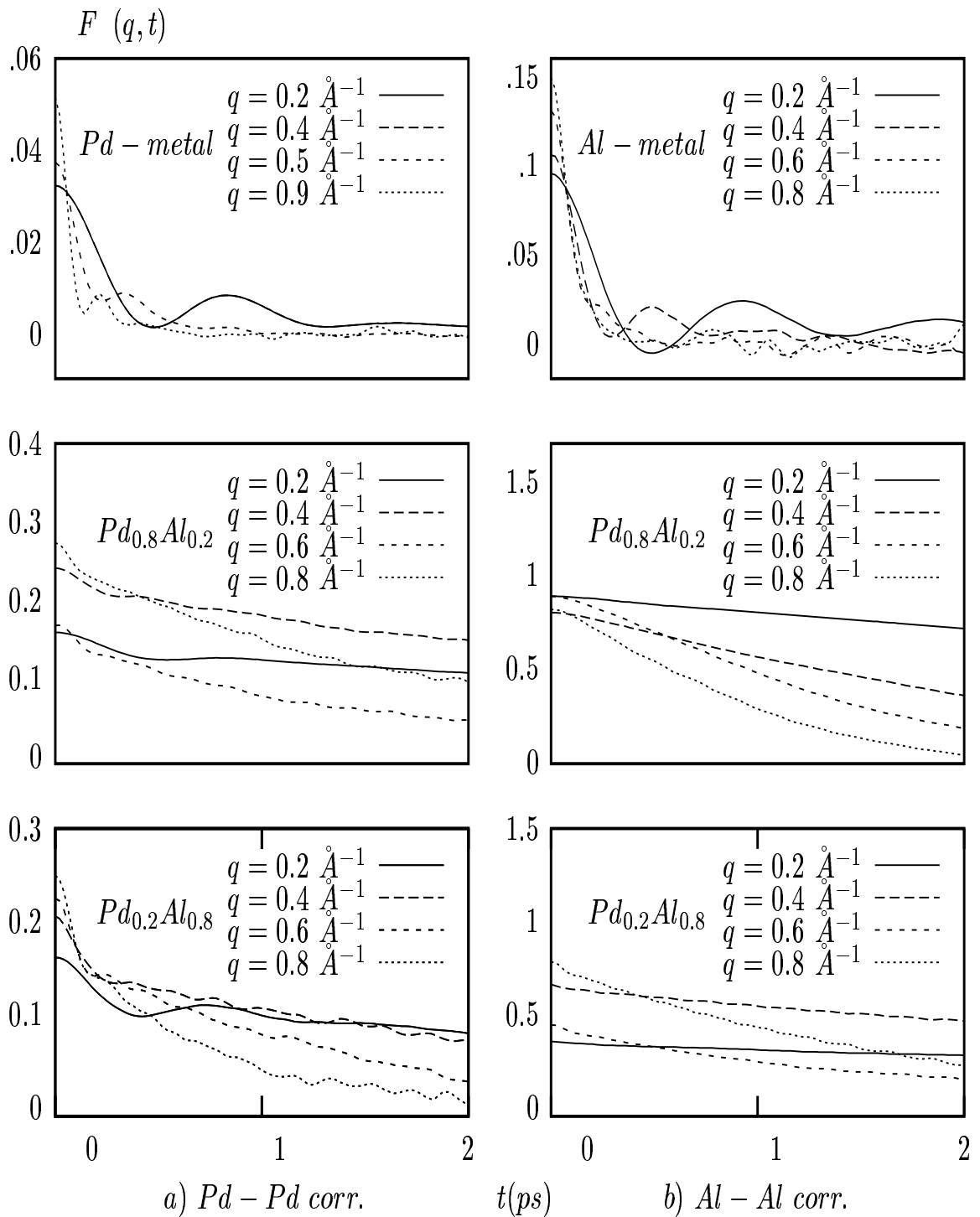
Figure 5.39: Hydrodynamic limit: (a) Pd-Pd partial intermediate scattering functions of liquid Pd metal, and $Pd_{0.8}Al_{0.2}$ and $Pd_{0.2}Al_{0.8}$ alloys from top to bottom respectively, (b) Al-Al partial intermediate scattering functions of liquid Al metal, and $Pd_{0.8}Al_{0.2}$ and $Pd_{0.2}Al_{0.8}$ alloys from top to bottom respectively($T = 1853\ K$).
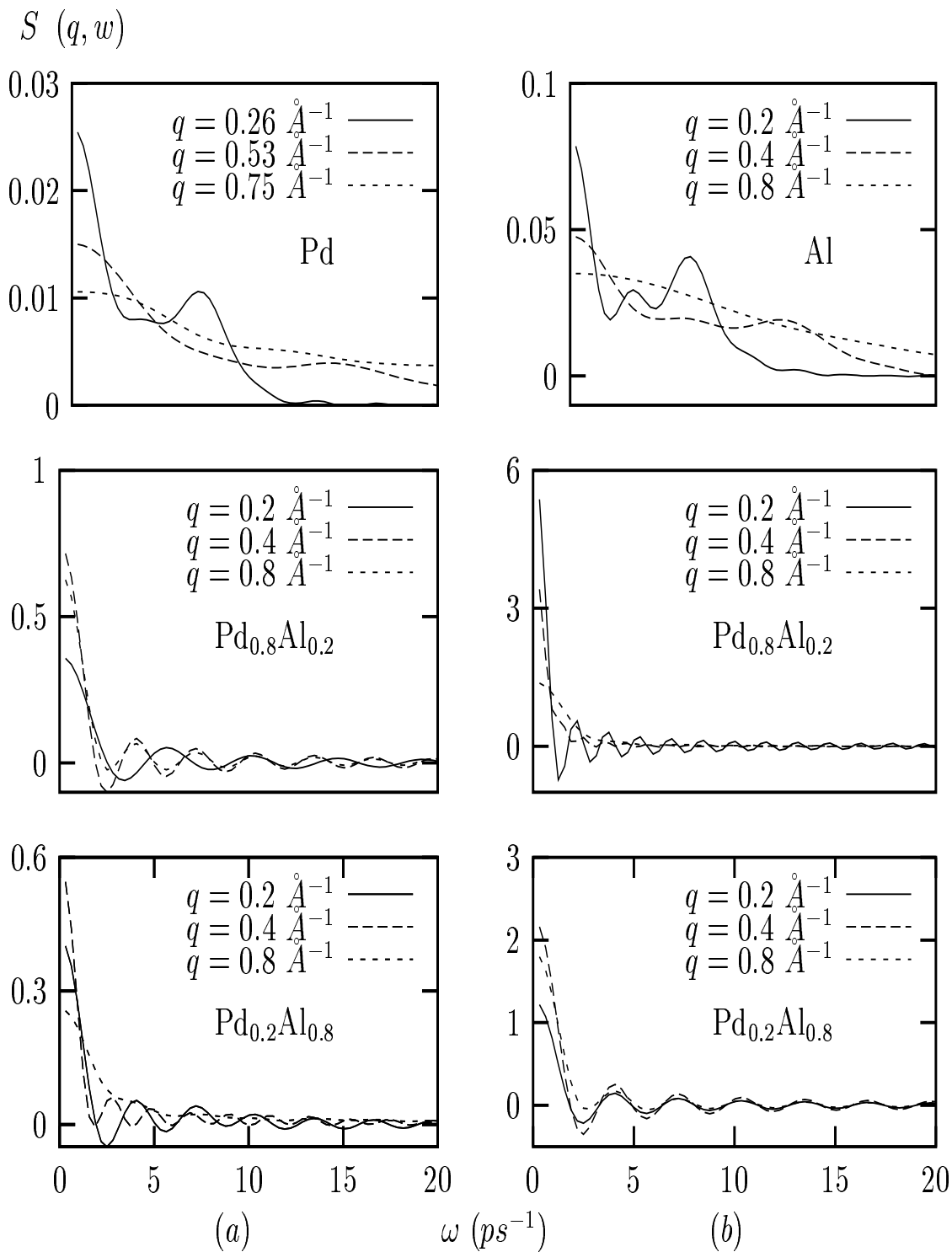
Figure 5.40: (a) Pd-Pd partial dynamic structure factors of liquid Pd, and $Pd_{0.8}Al_{0.2}$ and $Pd_{0.2}Al_{0.8}$ alloys, from top to bottom respectively, (b) Al-Al partial dynamic structure factors of liquid Al, $Pd_{0.8}Al_{0.2}$ and $Pd_{0.2}Al_{0.8}$ alloys, from top to bottom respectively, $T = 1850 \ K$.
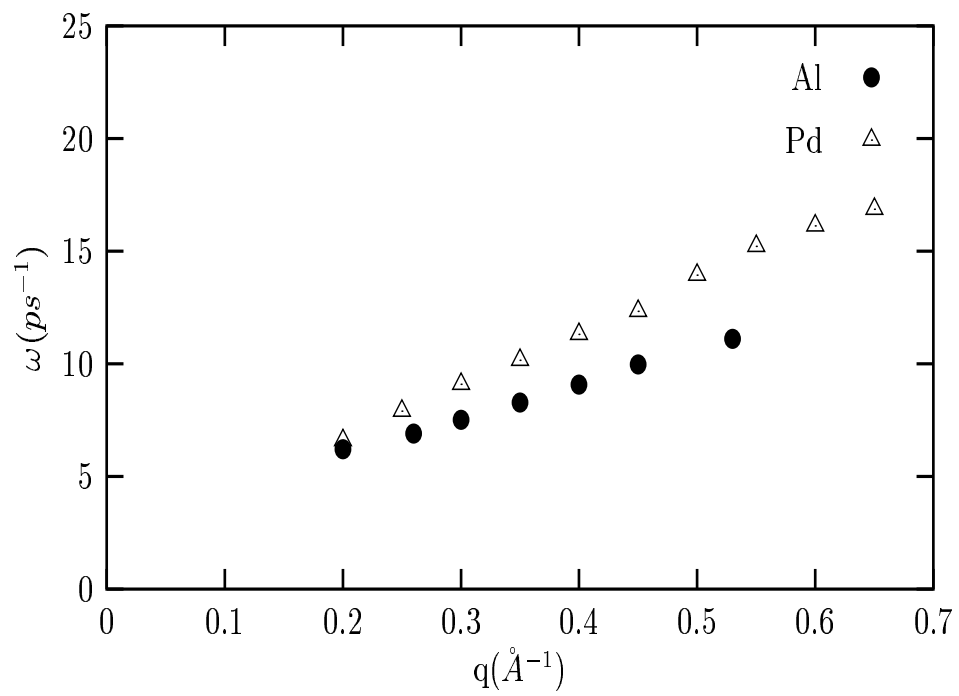
Figure 5.41: $\omega^{ij}(q)$ fast-sound modes of Pd and Al and T= 1850 K.

CHAPTER 6

CONCLUSION

Liquid Pd and Al metals and Pd-Al alloys in different concentrations are investigated in this work, by using MD simulation method. Sutton-Chen potential [62] is employed as inter-atomic potential with Q-SC parameters [64]. Rafii-Tabar and Sutton [63] formalism is employed for the alloy case.

In this work, a detailed investigation is carried out about dynamical properties of liquid Pd and Al, and their alloys in different concentrations. It is observed that, during the study of melting process, Q-SC parameters simulate well the Pd. Experimental melting point of Pd is 1827 K [1], and the simulated melting point of Pd is 1820 $\pm$ 5 K by using three reliable measures; namely, the difference in the pair distribution functions, discontinuity in enthalpy, and magnitude of diffusion coefficients.

Structure factor simulations show that there is agreement between the experimental [68] and simulated structure factors of Pd as shown in Table. 5.2. We can say that Q-SC parameters describe Pd well. Resulting from low melting temperature, simulated structure factors of Al show some differences from experimental ones at $T = 943$ K and $T = 1323$ K, as can be seen in Table. 5.3. The expected point of the first peak in the experimental structure factor is obtained correctly, and this implies that the lattice parameter fit of Q-SC potential agrees well in

the liquid phase also.

Our results for diffusion coefficients agree with the results of Alemany's calculations as it can be seen in Table. 5.4. There are several theoretical and MD simulation studies about diffusion coefficients of liquid Al. Theoretical results varies widely over a range. As it can be observed from Table. 5.4, Q-SC potential produces well the behavior of Al diffusion. Our findings are in agreement with previous MD data, but with the values higher than expected ones. Table. 5.4 lists self diffusion coefficients of Pd in Al. Diffusion coefficient is in the expected order. There is neither experimental nor simulated or theoretical data for Pd-Al alloy diffusion coefficients. However, the data produced in this work, can be a guiding criteria for future studies.

The viscosities have been calculated for liquid Pd and Al near their melting points by using Q-SC potential in the micro canonical ensemble (EVN). The present results for liquid Pd and Al given in Table. 5.5. The results illustrate that the computation of these transport properties are feasible and reliable. To the best of our knowledge, there is no experimental data about viscosity of Pd but there are a few simulation results or theoretical calculations [44]. Our calculations agree well with the calculation of Alemany [44]. For aluminum, experimental data for viscosity is scattered and our calculations are in the lower end of experimental or first-principle simulation results. The viscosities of $Pd_{0.8}Al_{0.2}$, $Pd_{0.6}Al_{0.4}$, $Pd_{0.4}Al_{0.6}$, and $Pd_{0.2}Al_{0.8}$ alloys have also been calculated in the present work. It is clearly seen that the viscosity of the alloy is increasing for increasing amounts of Pd in the Al.

84

The calculation of the intermediate scattering function is performed for two different limiting cases: the free particle limit which gives a Lorentzian shape for $F(q,t)$ functions, the other is the hydrodynamic limit. Hydrodynamic limit calculations lead to bulk modulus and compressibility calculations by using Eq. (5.10). Intermediate scattering function is a time-space correlation function, and it includes small exponential or sinusoidal terms which need to be calculated intensively. Bulk modulus is usually obtained by differentiating the pressure [77]. A comparison is given between $S(0)$ and $F(k, t \to 0)$ values in the hydrodynamic limit. There are some differences especially for the alloy case.

The dynamic structure factor calculations are performed for two different limiting cases. The free particle limit ($q \geq 1.0$ $\mathring{A}^{-1}$) simulations show that Pd-Pd correlation is much stronger than Al-Al correlation in both metallic and alloy cases. The hydrodynamic limit simulations show that, to the contrary, Al-Al correlation is stronger than Pd-Pd correlation especially in the alloy case. The peaks next to the central Rayleigh peaks are observed. The positions of these peaks define the $\omega(q)$ dispersion relations, namely the "fast-sound" modes [57, 77, 78]. These modes quickly disappear as the wave vector increases. Detailed information on this subject is given by Anento *et al.* [78, 119].

The present work is challenging as the first study of liquid Pd-Al alloy in literature. It can be said that MD simulation is an efficient way to investigate the material properties of matter. Although First-Principles techniques are more informative, Sutton-Chen many-body interaction model is still useful in the calculations but needs some improvements. We have seen in our study that

Sutton-Chen many-body interaction potential works well for liquid Pd but needs re-parametrization for liquid Al. Present properties of SC potential with Q-SC parameters show great promise to investigate liquid state properties but recent studies [85] show that Rafii-Tabar and Sutton's alloy case modification of Sutton-Chen potential needs new parametrization for the liquid alloy case studies. Pure metal parameters do not seem to be enough for studying alloys.

REFERENCES

[1] E. M. Savitskii, (1969) **Palladium Alloys**, (Monument Press, New York)

[2] V. A. Nemilov and A. A. Rudnitskii, **Izv. Sektora Platini AN SSSR**,27 (1952)

[3] M. van Lancker, (1967) **Metalurgy of Aluminum Alloys** (William Clowes and Sons, London)

[4] T. K. K. Mong, H.K. Lee, et al., Pnas **100**, 797 (2003)

[5] P., Chambon, Faseb J. Faseb. J. **10**, 940 (1996)

[6] L. M. De Luca, Faseb. J. **5**, 2924 (1991)

[7] P. Kastner, M. Mark and P. Chambon, Cell **83**, 859 (1995)

[8] K. Wallner, J. Roy, L. Harrison, J. Clin. Oncol. **14**, 449 (1996)

[9] A. V. D'Amico, C. N. Coleman, J. Clin. Oncol. **14**, 304 (1996)

[10] H. Ragde, J.C. Blasko, P.D. Grimm, et al., Cancer **80**, 442 (1997)

[11] Y. Zhang, T. Ozaki, M. Komaki, et al, Mater. Sci. Forum **426**, 3365 (2003)

[12] H. Abe, H. Uchida, Y. Azuma, et al., Nucl. Instr. Met. B **206**, 224 (2003)

[13] C. Fukuhara, A. Igarashi, J. Chem. Eng. Jpn. **36**, 530 (2003)

[14] M. P. Harold, B. Nair, G. Kolios, Chem. Eng. Sci. **58**, 2551 (2003)

[15] B.R. Evans, H.M. O'Neill, V.P. Malyvanh, I. Lee, J. Woodward, Biosensors and Bioelectronics **18**, 917 (2003)

[16] T. C. Huang, M. C. Wei, H.I. Chen, Separ. Sci. Technol. **36**, 199 (2001)

[17] V. Rousset et. al. Nanotechnology **7**, 144 (1996)

[18] A. Adamatzky, Int. J. Theor. Phys. **37**, 3069 (1998)

[19] A. Adamatzky, Adv. Mater. Opt. Electr. **7**, 263 (1997)

[20] D.Tolmachev, and A. Adamatzky, Adv. Mater. Opt. Electr. **6**, 191 (1996)

[21] A. Adamatzky, and D. Tolmachev, Adv. Mater. Opt. Electr. **7**, 135 (1997)

[22] A. Carrado, J. M. Sprauel, L. Barrallier, et al., Mater. Sci. Forum **426**, 3963 (2003)

[23] A. W. Szafranski, J. Phys. Condens. Mater. **15**, 3583 (2003)

[24] J. Moc, D. G. Musaev, K. Morokuma, J. Phys. Condens. Mater. A **107**, 4929 (2003)

[25] R. Djingova, P. Kovacheva, G. Wagner, B. Markert Sc. Total Environ. **308**, 235 (2003)

[26] M. Sambi, M. Petukhov, B. Domenichini et al., Surf. Sci. **529**, L234 (2003)

[27] G. Demarco, J. E. Garces, G. Bozzolo, Surf. Sci. **526**, 309 (2003)

[28] N. M. Taher, S S. Al Jabab, Dent. Mater. **19**, 54 (2003)

[29] C. Massen, T. V. Mortimer-Jones, R. L. Johnston, J. Chem. Soc. Dalton **23**, 4375 (2002)

[30] Jörg F. Löffler, Intermetallics **11**, 507-623 (2003)

[31] V. Matolin, V. Johanek, I. Stara, N. Tsud, K. Veltruska, Surf. Sci. **507**, 803 (2002)

[32] R. Hirschl, Y. Jeanvoine and J. Hafner, J. Phys. Cond. Mat. **13**, 3545 (2001)

[33] Toshiyuki Ohe and Sakae Uemura, Bulletin of the Chem. Soc. Jpn. **76**, 1423 (2003)

[34] J. M. Khalifeh and B. A. Hamad, Physica B **321**, 230 (2002)

[35] R. Szatanik and R. Pietrzak, Physica B **307**, 211 (2001)

[36] P. T. Huy, C. A. J. Ammerlaan, Physica B **308**, 408 (2001)

[37] N. Metropolis, S. Ulam, J. Am. stat. Ass **44**, 335 (1949)

[38] N. Metropolis, A. W. Rosenbluth, M. N. Rosenbluth, A. H. Teller, E. Teller, J. Chem. Phys. **21**, 1087 (1953)

[39] D. Knuth (1973), **The art of Computer Programming** [2nd edn.Chap. 3] (Addition-Wesley, MA)

[40] A. Rahman, Phys. Rev. **136A**, 405 (1964)

[41] R. Car, M. Parrinello, Phys. Rev. Lett. **55**, 2475 (1985)

[42] P. E. Blochl, M. Parrinello, Phys. Rev. B **45**, 9413 (1985)

[43] S. Bandyopadhyay, R. Venkatesh and R. V. Gopala Rao, Indian J. Pure Ap. Phy. **40**, 32 (2002)

[44] M. M. G. Alemany, C. Rey, L. J. Gallego, J. Chem. Phys. **109**, 5175 (1998)

[45] L. J. Munro, D. J. Wales, Faraday Discuss **106**, 409 (1997)

[46] G. R. Darling, M. Kay, S. Holloway, Surf. Sci. **400**, 314 (1998)

[47] P. Keblinski, D. Wolf, Phillpot SR, et al., Philos. Mag. A **79**, 2735 (1999)

[48] F. Baletto, R. Ferrando, A. Fortunelli, et al., J. Chem. Phys. **116**, 3856 (2002)

[49] Y. Sasajima, S Taya, R. Yamamoto, Mater. T. Jim. **34**, 882 (1993)

[50] M. Karabacak, S. Ozcelik, Z. B. Guvenc, Surf. Sci. **532**, 306 (2003)

[51] A. Gross., Phys. Rev. B **57**, 2493 (1998)

[52] P. V. Kumar, J. S. Raut, S. J. Warakomski, et al., J. Chem. Phys. **105**, 686 (1996)

[53] B. L. Holian, A. F. Voter, N. J. Wagner, et al., Phys. Rev. A **43**, 2655 (1991)

[54] M. Celino, G. DAgostino, V. Rosato, Mat. Sci. Eng. A-Struct. **204**, 101 (1995)

[55] P. Heino, P. Holloway, E. Ristolainen, J. Vac. Sci. Technol. A **18**, 1202 (2000)

[56] B. M. Axilrod and E. Teller, J. Chem. Phys. **11**, 299 (1943)
et al., J. Chem. Phys. **118**, 5484 (2003)

[57] J. P. Hansen, I. R. McDonald, (1986) **Theory of Simple Liquids**, (Academic Press, London)

[58] H. C. Andersen, J. Chem. Phys. **72**, 2384 (1980)

[59] S. Nosé, Mol. Phys. **52**, 255 (1984a)

[60] S. Nosé, J. Chem. Phys. **81**, 511 (1984b)

[61] M. W. Finnis and J. E. Sinclair, Phil. Mag. A **50**, 45 (1984)

[62] A. P. Sutton, J. Chen, Phil. Mag. Lett. **61**, 139 (1990)

[63] H. Rafii-Tabar and A. P. Sutton, Phil. Mag. Lett. **63**, 217 (1991)

[64] Y. Kimura, T. Çağın, and W. A. Goddard III (unpublished)

[65] Yue Qi, T. Çağın, Y. Kimura, and W. A. Goddard III, Phys. Rev. B **59**, 3527 (1999)

[66] T. Çağın, G. Dereli, M. Uludoğan, M.Tomak, Phys. Rev. B **59**, 3468 (1999)

[67] H. Feraoun, C. Esling, Superlattices Microst. **31**, 297 (2002).

[68] Y. Waseda, (1980) *The Structure of Non-Crystalline Materials - Liquids and Amorphous Solids* (Mc Graw Hill, New York)

[69] David M. Heyes, (1998) **The Liquid State: Application of Molecular Simulations** , (Wiley, West Sussex-England)

[70] M. S. Daw and M. I. Baskes, Phys. Rev. Lett. **50**, 1285 (1983)

[71] D. A. McQuarrie, (1976) **Statistical Mechanics**, (Harper and Row, New York)

[72] F. J. Cherne III and P.A. Deymier, Scripta Materialia, **45**, 985-991 (2001)

[73] J. Bosse, G. Jagucci, M.Ronchetti and W.Schirmacher, Phys. Rev. Lett. **26**, 3277 (1986)

[74] R. Hultgren, (1973) "**Selected Values of Thermodynamic Properties of the Elements**", (American Society of Metals, Metal Park, Ohio)

[75] G. Simmons and H. Wang, (1971) **Single Crystall Constants and Calculated Aggregate Properties:A Handbook** (Second Edition), (The M.I.T. Press, Cambridge)

[76] Takamichi Iida and Roderick I. L. Guthrie, (1993) **The Physical properties of Liquid Metals**,(Oxford Science Publications)

[77] I. Ebbsjö, T. Kinell, I. Waller Mol. Phys. **13**, 1865 (1980)

[78] N. Anento and J. A. Padró, Phys. Rev. E **64**, 021202-1 (2001)

[79] B. J. Alder and T. E. Wainwright, J. Chem. Phys. **31**, 459 (1959)

[80] D. Adams and G. Hills,(1981) **The Computer Simulation of Ionic Liquids** (Plenum, New York)

[81] M. P. Allen, D. Frenkel and J. Talbot, Comp. Phys. Repts. **9**, 301 (1989)

[82] W. G. Hoover, (1986) **Molecular Dynamics, Lecture notes in Physics**,(p-258) (Springer-Verlag. Berlin)

[83] W. C. Swope and H. C. Andersen, Phys. Rev. B **41**, 7042 (1990)

[84] K. Huang,(1987) **Statistical Mechanics**, (John Wiley, New York)

[85] M. Uludogan, (2003) "**Molecular-Dynamics Investigation of Pure Metals and Metal Alloys**", Ph. D. Thesis, (Middle East Technical University)

[86] M. Parinello and A.Rahman, Phys. Rev. Lett. **45**, 1196 (1980)

[87] M. Parinello and A.Rahman, J. Appl. Phys. **52**, 7182 (1981)

[88] M. Uludogan, (1996) "**Molecular-Dynamics Computer Simulations of Pure Metals and Metal Alloys**", M. Sc. Thesis, (Middle East Technical University)

[89] W. G. Hoover, (1991) **Computational Statistical Mechanics**, Elsevier, Amsterdam

[90] J. M. Haile, (1992) **Molecular Dynamics Simulation**, John Wiley and Sons, Inc., New York

[91] C. W. Gear, (1971) **Numerical Initial Value Problems in Odrinary Differential Equations**:Chapter 9, Prebtice Hall, Englewood Clifs, NJ

[92] M. P. Allen, D. J. Tildesley, (1997) **Computer Simulation of Liquids**, (Calerondon Press - Oxford).

[93] D. C. Rapaport, (1995) **The Art of Molecular Dynamics Simulation**, Cambridge Univ. Press, Cambridge

[94] D. J. Evans and G. Morris, (1990) **Statistical Mechanics of Nonequilibrium Liquids**, Academic, New York

[95] G. Cicotti and W. G. Hoover, Eds., (1986) **Molecular-Dynamics Simulation of Statistical-Mechanical Systems**, North-Holand, Amsterdam

[96] D. J. Adams, Chem. Phys. Lett. **62**, 629 (1979)

[97] K. Maeda, V. Vitek and A. P. Sutton, Acta. Met. **30**, 2001 (1982)

[98] Adrian P. Sutton, (1996) **Electronic Structure of Materials**, (Calerondon Press, Oxford).

[99] A. E. Carlsson and N. W. Aschroft, Phys. Rev. B **27**, 2101 (1983)

[100] G. J. Ackland, M. W. Finnis and V. Vitek, Phil. Mag. Lett. **18**, L153 (1988)

[101] K. Masuda and A. Sato, Phil. Mag. A **44**, 799 (1981)

[102] J. B. Pethica and A. P. Sutton, J. Vac. Sci. Technol. A. **6**, 2490 (1988)

[103] G. J. Ackland and V. Vitek, Phys. Rev. B **41**, 10324 (1990)

[104] M. T. Dove,(1993) **Introduction to Lattice Dynamics**, (Cambridge, Newyork)

[105] D. R. Poirier and G. H. Geiger, (1994) **Transport Phonemona in Material Processing.** (Warrendale), PA: The Minerals, Materials and Materials Society

[106] M. Dzugutov, Nature, **381**, 137 (1996)

[107] D. Alfe and M. J. Gillan, Phys. Rev. Lett. **81**, 5161 (1998)

[108] E. Helfand, Phys. Rev. **119**, 1 (1960)

[109] M. P. Allen and A. J. Masters, Mol. Phys. **79**, 435 (1993)

[110] W. R. D. Jones and W. L. Barlet, J. Inst. Met, **81**, 145 (1952-53)

[111] T. P. Yao and V. Kondic, J. Inst. Met, **81**, 17 (1952-53)

[112] T. P. Yao, Giesserei Techn-Wiss Beih **16**, 837 (1956)

[113] E. Rothwell, J. Inst. Met, **90**, 389, (1961-62)

[114] E. Gebhard and K. Detering, Z. Metallik **50**, 379 (1959)

[115] M. Canales and J. A. Padró, Phys. Rev. E **56**, 1759 (1997)

[116] H. J. Seeman and F. K. Klein, Z. Angew. (Math.) Phys. **19**, 368 (1965)

[117] P. G. de Gennes, Physica **25**, 825 (1959)

[118] A. Campa and E. G. D. Cohen, Phys. Rev. A **41**, 5541 (1990)

[119] N. Anento and J. A. Padró, Phys. Rev. B **62**, 11428 (2000-I)

[120] W. G. Hoover, Phys. Rev. A **31**, 1695 (1985)

[121] T. Çağın and B.M.Pettitt, Mol.Phys. **72**, 169 (1991)

[122] T.Çağın and B.M. Pettitt, Mol.Sim, **6**, 5 (1991)

[123] A. Coruh, M. Uludogan, M. Tomak, and T. Çağın, "Simulation Study of the Dynamical Properties of Pd and Al Transition Metals and Their Binary Alloys", submitted.

VITA

Ali ÇORUH was born in OF-TRABZON on March 20, 1966. After having graduated from OF Ş.A. Türkkan High School in 1983, he joined to the Physics Department of Karadeniz Technical University as a B. Sc. student. After receiving his B. Sc. degree in 1989, he received M. Sc. degree from the Department of Physics of Sakarya University. His M. Sc. thesis title is "Investigation of loss factors and cell constants in RF field-electrolitic solution interactions by using LRC circuit". In May 2000, he succeeded in the qualifying exam.

He was employed as a Physics teacher during the period of 1990-1993. Then, he employed as a research assistant in Sakarya University during the period of 1993-1999. Today, he is a research assistant in Middle East Technical University